

# High-Speed, High-Purity Separation of Gold Nanoparticle-DNA Origami Constructs using Centrifugation

Received 00th January 2012,

Accepted 00th January 2012

DOI: 10.1039/x0xx00000x

Seung Hyeon Ko,<sup>ab§</sup> Fernando Vargas-Lara,<sup>c</sup> Paul N. Patrone,<sup>ad</sup> Samuel M. Stavis,<sup>a</sup> Francis W. Starr,<sup>f</sup> Jack F. Douglas,<sup>c</sup> J. Alexander Liddle<sup>a\*</sup>

DNA origami is a powerful platform for assembling gold nanoparticle constructs, an important class of nanostructure with numerous applications. Such constructs are assembled by the association of complementary DNA oligomers. These association reactions have yields of < 100 %, requiring the development of methods to purify the desired product. We study the performance of centrifugation as a separation approach by combining optical and hydrodynamic measurements and computations. We demonstrate that bench-top centrifugation is a simple and efficient method of separating the reaction products, readily achieving purities of > 90 %. The gold nanoparticles play a number of critical roles in our system, functioning not only as integral components of the purified products, but also as hydrodynamic separators and optical indicators of the reaction products during the purification process. We find that separation resolution is ultimately limited by the polydispersity in mass of the gold nanoparticles and by structural distortions of DNA origami induced by the gold nanoparticles. Our study establishes a methodology for determining the design rules for nanomanufacturing DNA origami-nanoparticle constructs.

## 1. Introduction

Structural DNA nanotechnology has evolved since the early 1980s when Nadrian Seeman first proposed that DNA molecules could be used as nanoscale building blocks.<sup>1</sup> A significant acceleration has occurred recently, following the demonstration of high-yield, discrete, readily-functionalized DNA nanostructures by Rothemund<sup>2</sup> and others.<sup>3-6</sup> The field has now reached a critical juncture, with practical applications becoming a real possibility as techniques for assembling more complex, multifunctional nanostructures are developed. For this potential to be realized, however, a number of nanomanufacturing issues must be addressed, including the relatively high rate of assembly errors, slow assembly process, limited scale, and high cost of starting materials.<sup>7,8</sup> A number of groups have made progress in some of these areas, with improvements in the time taken to assemble complex structures<sup>9</sup> and the development of novel schemes to increase the scale and speed of the production of DNA nanostructure component parts.<sup>10</sup>

Despite these advances, obstacles to widespread deployment of DNA-based assembly processes remain. In particular, one of the most attractive features of structural DNA nanotechnology – its ability to precisely organize disparate nanomaterials into heterogeneous nanostructures – is difficult to take advantage of due to the lack of suitable, scalable purification methods. These methods are essential because the attachment yield of nano-components for any target nanostructure is less, often much less, than 100 %.<sup>11</sup> The problem of separating the desired product from unreacted or incompletely reacted species, and mis-assembled structures becomes compounded as more species of nanostructure, with potentially different attachment mechanisms, are engineered into these complexes. Practical solutions to such multidisciplinary problems lie at the intersection of biology, chemistry, physics and engineering, motivating a systems-level approach – combining theory and

experiment – to designing and fabricating structures with the desired functionality at high yields and purities.

In contrast, the most commonly used method for separating well-folded DNA nanostructures from other by-products, agarose gel electrophoresis, has not been optimized at the system level, and suffers from severe technical limitations in the present context.<sup>12</sup> First, only a small ( $\approx 10 \mu\text{L}$ ,  $\approx 1$  pico mole) quantity of sample can be loaded onto a gel. Then, there is a need for a reference material against which to calibrate the electrophoretic mobility of the products. Further, in separations of nanohybrid structures, such as AuNPs attached to DNA origami, the electrophoretic mobility of the construct is essentially the same as that of the origami, leading to a lack of resolution in the gel that makes effective separations all but impossible (Fig. S1).<sup>13,14</sup> Following separation, recovery yields of the products after extraction from the gel pieces when using electroelution or a freeze-squeeze column are less than 100 %, and the desired structures may also be damaged. Finally, it may be difficult to remove residual gel from the products.

These limitations have led to the search for alternative separation/purification methods. Centrifugation in various forms<sup>15</sup> has a long history in the preparation and analysis of large biomolecules<sup>16</sup> and can achieve very high resolution.<sup>17</sup> Shih and co-workers recently reported the use of ultracentrifugation (using accelerations of up to  $300\,000 \times g$ ) in a glycerol gradient to separate well-formed DNA origami structures from excess staple strands and origami multimers.<sup>18</sup> Centrifugation separation has also been actively used for sorting nanostructures including nanoparticles<sup>19-23</sup> and carbon nanotubes (CNTs). In the latter case, the precise separation of CNTs according to their electrical and structural properties has been shown.<sup>24-27</sup> However, until now, the effectiveness of rate-zonal centrifugation for the separation of more complex constructs involving heterogeneous nanomaterials has not been demonstrated.

Here, we show that rate-zonal centrifugation in a basic, bench-top microcentrifuge is a simple method for separating DNA origami-AuNP constructs from unwanted nanostructures and reactants, and that it further allows the extraction of specific, and even multiple, target products with high efficiency. In our design for nanomanufacturing approach, we use gold nanoparticles, arguably one of the most important constituents of many DNA-based heterostructures,<sup>28-37</sup> as a multifunctional component that: confers useful optical properties, serves as a means of separating out the target constructs, and also acts as a visual marker enabling facile extraction of the desired product. Simultaneously, we choose the configuration of the AuNP binding sites to maximize binding yield, and the centrifugation medium to simplify product extraction and purification. In this way, we demonstrate that rate-zonal centrifugation, at modest accelerations in a bench-top microcentrifuge, is an efficient, scalable separation technique, with high recovery yields that delivers purities of > 90 %.

Rate-zonal centrifugation separation is performed by loading the sample solution in a narrow ( $\approx 0.5$  mm) single layer on top of a gradient medium inside a 2.0 mL tube. The tube is centrifuged under a combination of acceleration and gradient medium density and viscosity, chosen in this case, to achieve separation in a few hours in a microcentrifuge. The objects sediment through the medium under the collective influence of three forces: centrifugal force ( $F_C$ ), ( $\propto$  mass), buoyant force ( $F_B$ ), ( $\propto$  volume), and drag force ( $F_D$ ), ( $\propto$  hydrodynamic radius). Ideally, the resultant of these three forces should be sufficiently different for different objects to yield distinct (i.e., maxima more than one standard deviation apart) bands that can then be extracted from the tube. We note that the large density of the origami-AuNP constructs precludes the use of isopycnic centrifugation. That method relies on the construction of a density gradient through which objects sediment until they reach a position where the density of the surrounding medium is the same as that of the object itself. Isopycnic centrifugation has been commonly used for separating biomolecules and, more recently, carbon-based nanomaterials, but any cluster or rational assembly of more dense nanoparticles (e.g., gold) cannot be sorted using this technique due to the lack of separation media with sufficiently high density. While the use of high-density AuNPs precludes isopycnic separation, it does make it possible to engineer the mass of the desired product thereby enabling efficient separations to be performed.

In this work, we investigate rate-zonal centrifugation in an iodixanol gradient as a means to separate a variety of AuNP-DNA constructs and examine the effect of AuNP size, number, and the complex interactions between nanoparticles and origami on the performance of this approach. The ability to resolve different constructs depends on the details of the hydrodynamic behaviour and mass of the constructs. We also find that the DNA origami-AuNP system exhibits conformational changes due to Au-DNA interactions, with important implications not only for the performance of this separation and purification method, but also for the design, synthesis and application of such constructs. We employ dynamic light scattering (DLS) to measure the hydrodynamic size,  $R_H$ , of the various constructs and use simulations to explain the observed non-monotonic variation in  $R_H$ , with increasing AuNP size and number.

## 2. Results and discussion

### 2.1 Separation of DNA Origami-AuNP complexes

We fabricated  $n$ AuNP-DNA origami ( $n = 1, 2, \text{ and } 3$ ; the number of AuNP bound onto DNA origami) using rectangular DNA origami ( $70 \text{ nm} \times 100 \text{ nm}$ ) as a template. Each binding location for AuNPs consists of three hybridizing staple strands, modified by extending them with 22 adenines (A) at predefined positions. AuNPs were fully covered with single strands of 18 thymines (T) (di-thiolated at the 5'-end), in order to avoid aggregation of AuNPs at the high concentration of  $\text{Mg}^{2+}$  needed to stabilize the origami. We constructed three different patterns ( $n = 1, 2, \text{ and } 3$ ) of AuNPs on DNA origami by mixing AuNP solution with the origami template solution at a stoichiometry of 2:1 (AuNP : binding site), and cooling overnight from  $37^\circ \text{C}$  to room temperature. We purified these samples directly by centrifugation separation without any pre-treatment.

We performed rate-zonal centrifugation of  $n$ AuNP-origami using a nine-layer density/viscosity gradient (made with 10 %, 15 %, ..., 50 % mass concentration of iodixanol in tris(hydroxymethyl)aminomethane-acetate-(ethylenediamine tetraacetic acid) (1X TAE/ $\text{Mg}^{2+}$ ), Table S1) and centrifugation in a bench-top microcentrifuge at an acceleration chosen to separate constructs with a given AuNP size within a period of < 270 min. We used a swing-bucket rotor for centrifugation. In this configuration, the centrifuge tubes swing out to a horizontal position during rotation, thus maximizing the distance the materials travel through the separation medium and eliminating the band distortion that can occur in fixed-rotor systems in which the separation medium slides down the wall of the centrifuge tube. As a gradient material, we chose iodixanol (density =  $1.32 \text{ g}\cdot\text{cm}^{-3}$  for 60 % mass concentration in water, viscosity  $\approx 11 \text{ mPa}\cdot\text{s}$ ) which is non-ionic and has good solubility in water. This material also exhibits minimal hydrogen bonding interactions, and can therefore be readily separated from DNA, unlike glycerol. We also note that it is *necessary* to use a gradient medium to avoid convection currents which tend to destroy stability of the bands (control experiments are shown in Figure S2).<sup>38,39</sup>

To demonstrate the separation efficacy of centrifugation, we tested various AuNP-DNA origami constructs using AuNPs with nominal diameters of 5 nm, 10 nm, 15 nm, 20 nm, and 30 nm with actual core-size distributions of the AuNPs measured by transmission electron microscopy (TEM). Fig. 1 shows the evolution of the sedimentation distribution for 10 nm  $n$ AuNP-DNA origami constructs ( $n = 1, 2, \text{ and } 3$ ). The plasmon absorption of the AuNPs functions as a visual indicator of the separation process, obviating the need for fraction-by-fraction analysis of the tube contents to determine construct location.<sup>18</sup>

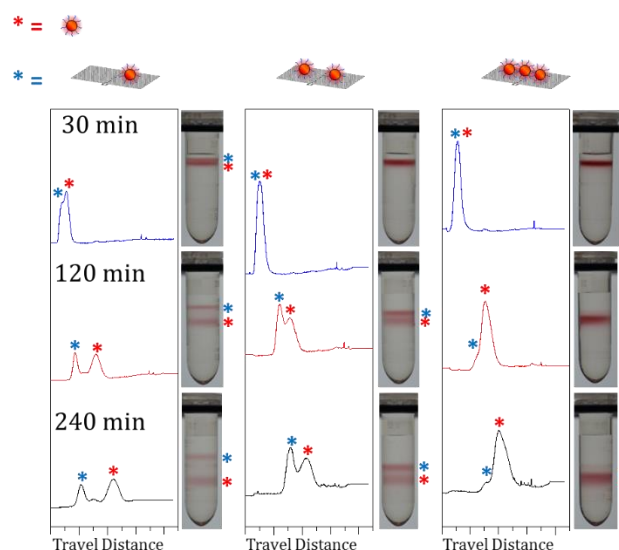


Fig. 1 Evolution of sedimentation distribution of various constructs of  $n=10$  nm AuNP-DNA origami at different time intervals as indicated by images of centrifuge tubes and corresponding image density traces.

We monitored band separation by using the intensity of the absorption as a function of position along the centrifuge tubes at different time intervals. After 270 minutes of centrifugation at  $850 \text{ rad}\cdot\text{s}^{-1}$  ( $68\,600 \text{ m}^2\cdot\text{s}^{-2}$ ,  $7\,000 \times g$ ), several distinct red bands were clearly visible in the centrifugation tubes as shown in Fig. 2a. The performance of the separation was investigated by recovering each band from the medium by pipetting, followed by buffer exchange using centrifuge filtration, followed by inspection of the constructs by scanning electron microscopy (SEM) (Fig. 2b-d). Analysis of the SEM images reveals purities of better than 90 % for each fraction: f1 is ( $96.1 \pm 0.5$ ) % 1AuNP-origami, f2 is ( $94.6 \pm 1.0$ ) % 2AuNP-origami, and f3 is ( $92.9 \pm 1.3$ ) % 3AuNP-origami. Unless otherwise noted all measurements are reported as (average  $\pm$  one standard deviation). Additional SEM images of larger areas for each fraction are provided in the supporting information (Fig. S4a-c). In addition to the high purity of each fraction, the process is highly efficient (Fig. S5), with the amount of material recovered close to the starting amount – suitable for immediate application or enabling further fabrication steps.

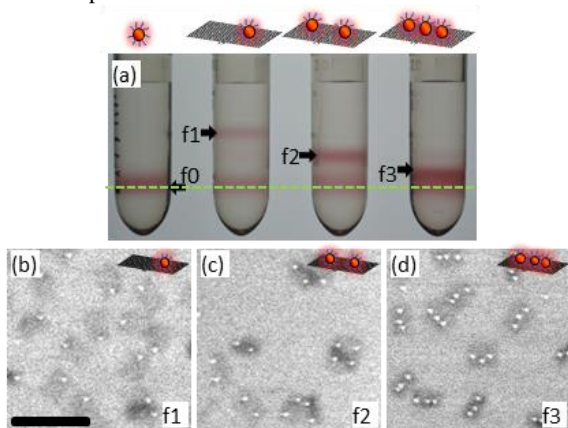


Fig. 2 Separation of  $n=10$  nm AuNP-DNA origami. (a) Photograph of centrifuge tubes containing different constructs after spinning for 270 min. at  $850 \text{ rad}\cdot\text{s}^{-1}$  ( $8\,100 \text{ rpm}$ ,  $68\,600 \text{ m}^2\cdot\text{s}^{-2}$ ,  $7\,000 \times g$ ). (b)-(d) Typical SEM images of different fractions of AuNP-origami constructs as labelled in (a). Schematics of the target product are shown for each tube. The fraction labelled f0 corresponds to free AuNPs. The SEM scale bar is 200 nm.

As shown in Fig. 2a, the band corresponding to 3AuNP-origami fraction, f3, is adjacent to that of the fraction f0, corresponding to free AuNPs, making separation difficult in this case. It is therefore important to understand the degree to which constructs can be engineered to enable the separation of different constructs from one another and from the starting materials.

During centrifugation, constructs with the same sedimentation coefficient,  $s$ , travel through the medium as a narrow band:  $s$  depends on the mass, volume and hydrodynamic size of the constructs according to the Svedberg equation,

$$s = \frac{dr/dt}{\omega^2 r} = \frac{m - V\rho_s}{6\pi\eta_s R_H} \quad (1)$$

where  $\omega$  is the angular velocity,  $r$  is the distance of the object from the rotation axis,  $m$  is the mass of the object,  $R_H$  is the hydrodynamic radius of the object,  $V$  is volume of the object,  $\eta_s$  is the dynamic viscosity of the fluid, and  $\rho_s$  is the density of the fluid. Equation (1) is derived in the Supporting Information. In the case of a density gradient medium, both  $\rho_s$  and  $\eta_s$  are functions of  $r$ .  $R_H$  may also vary

with  $r$ , depending on the interaction of the DNA with the gradient medium. We neglect this latter effect in our analysis because we expect it to influence only the apparent thickness of the shell of single-stranded DNA (ssDNA) on the AuNPs, but not the origami, which is a much more constrained structure. As expected, the sedimentation velocity of 10 nm  $n$ AuNP-DNA origami constructs increases with  $n$ , while the band of free AuNPs – having the largest  $m/R_H$  ratio – sediments most rapidly through the medium. The hydrodynamic size of the AuNPs increases dramatically upon binding to the free origami, which has an  $R_H$  of ( $35.0 \pm 1.4$ ) nm. This more than compensates for the mass added by the origami.

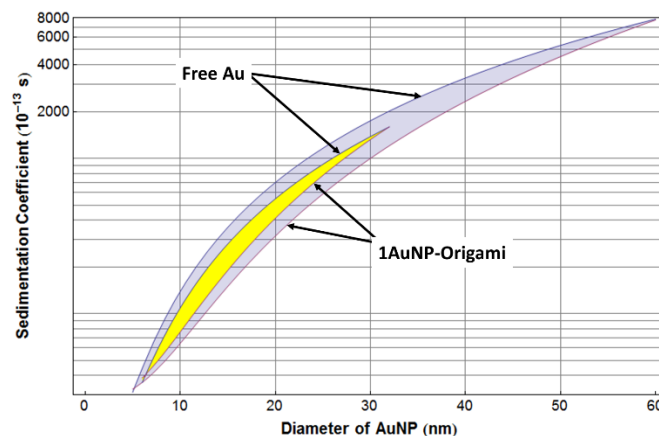


Fig. 3 Sedimentation coefficient versus particle size for free gold nanoparticles and 1AuNP-origami constructs. The large shaded area represents the range of particle sizes over which separations between free AuNPs and AuNP-origami constructs can be achieved, assuming a monodisperse size distribution. The small shaded area represents the range of particle sizes over which separations can be achieved, assuming a size distribution which varies between  $\pm 10\%$  about the average.

We estimate our ability to resolve the different species into separate bands using the sedimentation coefficients calculated for each construct from equation (1) to estimate the distance travelled during centrifugation. As a starting point for this calculation, we assume that the hydrodynamic radius of constructs containing  $n$ AuNPs is constant, dominated by the size of the DNA origami, and is unaffected by the number of attached AuNPs. We expect this naïve assumption to be reasonably good for particles that are small relative to the origami, but to break down at larger particle sizes. We calculate the mass of the constructs using the known densities of DNA and Au and the designed and measured sizes of the DNA and Au components, respectively. We compare our estimates to data obtained from “centrifugrams” – measurements of optical density taken from digital photographs – as a function of  $r$  (Fig. S6). Analysis of the resulting curves allows us to measure the centre and width of each band and hence determine the mean and standard deviation of the normalized travel distance of each construct. We note that the width (FWHM) of the observed bands is controlled by that of the AuNP size, and hence mass, distributions – both the initial width of the solution ( $\approx 0.5$  mm) upon loading in the centrifuge tube and diffusion occurring during centrifugation are minor contributors.<sup>40</sup>

Fig. 3 shows the results of calculations of the sedimentation coefficients for free gold nanoparticles and 1AuNP-origami constructs versus nominal particle size for a flat viscosity profile and infinite tube length (Plots for Ag and CdSe nanoparticles are included in the SI (Fig. S18) for comparison). A plot for our actual experimental conditions is shown in the SI (Fig. S19). Although the absolute band positions change with the details of the viscosity

profile, the relative positions are unchanged. Separation of constructs with purities > 90 % is not possible for nominal particle diameters smaller than 6 nm or larger than 27 nm because the change in sedimentation coefficient caused by the addition of the particle to the origami for small particles, or the origami to the particle for large particles, is less than the variation in sedimentation coefficient (which corresponds to band width) due to particle polydispersity.<sup>41</sup>

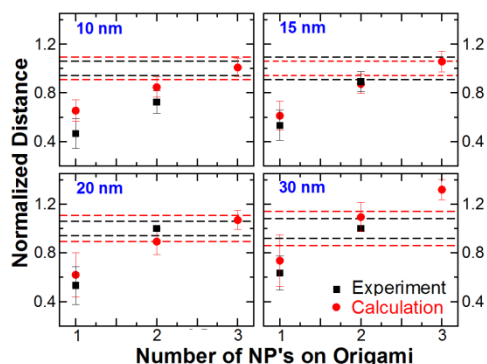


Fig. 4 Band displacement distances following centrifugation of  $n$ AuNP-DNA origami normalized against those of the corresponding free AuNP. The dashed lines correspond to the normalized free AuNP travel distance variations (red circles – calculated, black squares – measured). The experimental distances were determined from the peaks in densitometry traces of digital images of the centrifuge tubes. The experimental error bars correspond to the standard deviations of the peaks (derived from the full-width half-maxima, assuming an approximately Gaussian distribution). The calculated error bars are determined by using the experimentally determined standard deviations of the particle size distributions derived using Gaussian fits to the TEM data (extensive measurements of similar AuNPs show quite complex distributions) to estimate the range in travel distances for Au NPs of different sizes. The error bars are normalized to the travel distances of their respective peaks.

Fig. 4 shows a plot of the normalized calculated and experimental centrifugation peak locations and widths for each set of constructs containing 10 nm, 15 nm, 20 nm and 30 nm AuNPs (Fig. S7-S16). By estimating the area under each peak and taking account of the total number of AuNPs present, we are able to obtain a qualitative indication of the yield of each fraction in cases where a mixture of products is generated. This yield estimation method is a useful diagnostic tool for optimizing assembly conditions. A comparison of the measured *vs.* calculated sedimentation distances indicates that, although the calculations capture the overall trends reasonably well, there are significant discrepancies with the experimental data. In particular, while the experimental normalized travel distances generally lie below the estimated ones, those measured for both the 15 nm and 20 nm 2AuNP-origami do not follow this trend. Since the mass of each construct is well defined within the limits discussed above, variations in the hydrodynamic radius are the most likely cause of changes in the sedimentation behaviour. In order to investigate this effect further, we compared the measured and simulated hydrodynamic radii of AuNPs, before and after DNA attachment, and of the various  $n$ AuNP-origami constructs (Fig. 5).

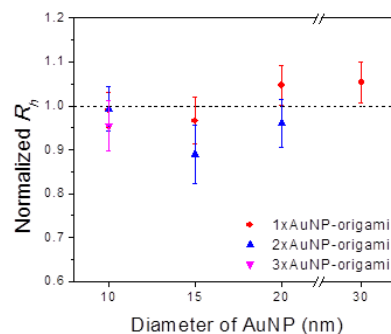


Fig. 5 Hydrodynamic radii of AuNP-origami constructs in buffer measured by dynamic light scattering. Hydrodynamic radii of the constructs are normalized by the radius of free origami ( $(35.0 \pm 1.4)$  nm). The bars represent one standard deviation for variation of different batches (measurements taken from at least three different samples prepared on three different days).

## 2.2 Simulation of $R_H$ of Origami, ssDNA-AuNPs and AuNP-Origami Complexes

It is apparent from Fig. 5 that the AuNPs have a significant influence on the hydrodynamic radius of the constructs. Rather than simply remaining constant or increasing with the addition of more or larger AuNPs, we observe a non-monotonic variation in  $R_H$  as more AuNPs are added. This effect is pronounced for the 15 nm and 20 nm 2AuNP-origami constructs – consistent with our observations from Fig. 4. To explore this counter-intuitive phenomenon, we first use molecular dynamic simulations of coarse-grained models of DNA-functionalized Au nanoparticles, origami, and  $n$ AuNP-origami complexes to determine their respective structures. We then apply the ZENO program<sup>42-44</sup> for computing the hydrodynamic radii of complex-shaped particles to calculate the hydrodynamic radii of each species. ZENO is capable of computing the  $R_H$  of objects of complex and essentially arbitrary initial specified geometry, a task not possible by analytic computation, and currently infeasible by molecular dynamics simulations for particles having the size and intricate shape of the AuNP-origami complexes (Even the  $R_H$  of an individual flexible chain cannot currently be accurately calculated analytically).<sup>42,43,45</sup>

The structure of the origami, DNA-functionalized Au nanoparticles and  $n$ AuNP-origami complexes is determined using a coarse-grained model reported previously.<sup>46, 47</sup> We represent DNA strands as a chain of “beads”, connected by non-linear springs. In the following figures, the ssDNA attached to the AuNP is shown as blue spheres, the double-stranded DNA (dsDNA) in the origami is shown as grey spheres, and the AuNP cores are depicted as red spheres. The AuNP model used here is a small modification of the one introduced in references 42-44, and the origami molecular model corresponds to a modified version of that presented in reference 46.

We treat the ssDNA as a chain with a distance between bases of  $\approx 0.65$  nm and employ a Kremer-Grest (KG) potential<sup>48</sup> to model the interaction between bases. This potential is described by the sum of a Weeks-Chandler-Andersen (WCA) potential ( $U_{WCA}$ ) accounting for non-bonded, inter-molecular excluded-volume interactions and short-range repulsion (Eq. 2), and a finitely extensible non-linear elastic ( $U_{FENE}$ ) potential to capture intra-molecular interactions (Eq. 3). A three-body angular potential (Eq. 4) accounts for the chain stiffness and determines the persistence length ( $\approx 2$  nm for ssDNA at the salt concentration used here).<sup>49</sup>

$$U_{WCA}(r) = \begin{cases} 4\epsilon \left[ \left( \frac{\sigma}{r} \right)^{12} - \left( \frac{\sigma}{r} \right)^6 \right] + \epsilon, r < 2^{\frac{1}{6}} \sigma \\ 0, r > 2^{\frac{1}{6}} \sigma \end{cases} \quad (2)$$

$$U_{FENE}(r) = -\frac{1}{2} k_{FENE} \left( \frac{3}{2} \sigma \right)^2 \text{Log} \left[ 1 - \left( r / \left( \frac{3}{2} \sigma \right) \right)^2 \right] \quad (3)$$

$$U_{linear}(\theta) = k_{linear} [1 + \cos(\theta)] \quad (4)$$

The parameter  $\epsilon$  defines the energy scale and is taken to be approximately  $2.5 \text{ kJ mol}^{-1}$  (equivalent to  $k_B T$ ), while  $\sigma$  determines the length scale (bead size) and is taken to be  $\approx 0.65 \text{ nm}$  – the effective length of a single nucleotide in fully extended ssDNA.  $k_{FENE}$  is  $30 \epsilon$  and  $k_{linear}$  is  $6 \epsilon$ , to match the persistence length,  $L_P = k_{linear} \sigma / 2k_B T \approx 2 \text{ nm}$ , of ssDNA.<sup>50</sup>

The AuNPs are also modeled using a WCA potential, but with the origin shifted to move the repulsive interaction to the AuNP particle surface. The AuNPs are functionalized with a number of ssDNA strands that depends on both the AuNP size and the salt concentration used during the attachment process.<sup>51–53</sup> We then perform molecular dynamics simulations for  $10^8$  time steps to equilibrate the system and apply the ZENO program to compute the  $R_H$  for a set of  $10^3$  configurations for each system: DNA-grafted AuNPs, origami, and  $n$ AuNP-origami complexes.  $R_H$  is determined as the peak value in the probability density function obtained from the  $10^3$  configurations. The  $R_H$  values computed for the functionalized AuNPs are shown in Fig. 6 and are in good agreement with our measured values of  $R_H$ , supporting the model and our choice of input model parameters such as DNA grafting density and DNA molecular dimensions.

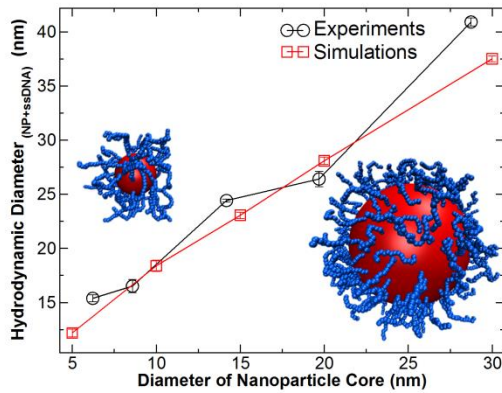


Fig. 6 Comparison of measured and simulated hydrodynamic radii for ssDNA-functionalized AuNPs of nominal radii 5 nm, 10 nm, 15 nm, 20 nm and 30 nm. The experimental vertical bars represent the standard deviation of 3 separate DLS measurements and the vertical bars in simulation data represent the standard deviation obtained from the distribution of the  $10^3$  simulations performed for each particle type.

At the  $\text{Mg}^{2+}$  concentrations needed to stabilize the origami, citrate-stabilized Au nanoparticles are not stable against aggregation.<sup>54</sup> However, a high coverage of poly-T results in steric interactions sufficient to prevent salt-induced aggregation.<sup>55</sup> As noted above, the density of ssDNA on the surface of the AuNPs decreases with increasing particle radius, meaning that the particles become, in principle, less stable against aggregation as they become larger – consistent with our and other<sup>56,57</sup> observations that preparing stable suspensions of ssDNA-functionalized AuNPs is more challenging for larger nanoparticles. We also expect that the attractive interaction

between the DNA and the AuNP surface becomes stronger with increasing NP size,<sup>58</sup> and can result in binding<sup>59</sup> and attractive interactions with dsDNA.<sup>60</sup> These latter two facts motivate the inclusion of an attractive interaction between the AuNP surface and the dsDNA of the origami in the potentials.

We model the origami ( $\approx 100 \text{ nm} \times 70 \text{ nm} \times 2 \text{ nm}$ ) used in these experiments as a rectangle of  $154 \times 108$  spheres in the  $x$  and  $y$  directions respectively, connected *via* the FENE potential. Since the origami is not elastically isotropic, we use different spring constants in the two directions ( $k_x = 90 \epsilon$  and  $k_y = 3 \epsilon$ , respectively). The net result is a persistence length,  $l_{p\text{-dsDNA}}$  of approximately  $59 \text{ nm}$  along  $x$  (corresponding to that of dsDNA) and a stiffness ratio of 15 between the  $x$  and  $y$  directions (an estimate designed to account for the distance between and flexibility of the crossovers between the dsDNA strands). In order to account for the shear stiffness of the origami, we introduce a potential,  $U_{perp}$ , (Eq. 5) that depends on the angle formed by three neighboring beads; two beads that belong to one chain, and one bead from the adjacent chain. In addition, we introduce a weak attractive interaction between the origami and the AuNP using a Lennard-Jones potential (Eq. 6) truncated at  $r = 2.5 \sigma$  and model two cases, with characteristic energies of 0 and  $\epsilon$ , respectively, representing the likely range of interaction strengths. Finally, we mimic the attachment of the DNA-functionalized AuNP to the origami by introducing a harmonic potential (Eq. 7) between the last bead of the ssDNA chains on the NP and the beads on the origami.

$$U_{perp}(\alpha) = \frac{k_{perp}}{2} \left( \alpha - \frac{\pi}{2} \right)^2 \quad (5)$$

$$U_{LJ}(r) = 4\epsilon \left[ \left( \frac{\sigma}{r} \right)^{12} - \left( \frac{\sigma}{r} \right)^6 \right] \quad (6)$$

$$U_{harm}(r) = \frac{k_{harm}}{2} (r - r_0)^2 \quad (7)$$

The interaction between DNA and the DNA-grafted AuNPs in solution is a complex problem involving a number of competing interactions, which depend on solution conditions – such as pH and salt concentration – DNA sequence, DNA chain mass, the form of the hybridized DNA, and AuNP size. Apart from the naturally attractive interactions between the hybridizing complementary strands of the DNA chains grafted onto the AuNPs and those extending from the origami, we note that DNA molecules themselves can have appreciable, attractive, non-specific interactions with Au and many other interfaces. In particular, ssDNA has been found to bind strongly to macroscopic planar Au interfaces:<sup>61</sup> an effect attributed by Herne and Tarlov to the strong interaction between the (polarizable N) atoms of the DNA nucleotides with the AuNP. On the other hand, Murphy et al.<sup>62,63</sup> have found that oligomeric ssDNA *does not* adsorb onto small AuNPs (14 nm) within the range of our measurements. The size of the AuNP thus influences the strength of the binding interaction of the ssDNA with the AuNP. This effect has recently been studied both experimentally<sup>64</sup> and computationally<sup>65</sup> in the context of the adsorption of proteins on small AuNPs. In particular, the simulations of Feng et al.<sup>65</sup> emphasize the predominant role of the interaction of polarizable protein atoms (N, O, C) with the Au in understanding this fundamental NP size effect on molecular binding. Such interactions can also be expected to be prevalent in DNA through the presence of the polarizable N atoms in the nucleotides, consistent with the suggestion of the important role of this non-specific interaction between N and Au by Herne and Tarlov.

Murphy and coworkers<sup>62,63,66</sup> emphasize that the binding of ssDNA to Au is sequence dependent because of the influence of DNA sequence on the ‘coiled’ nature of DNA. Any factor influencing the persistence length, or equivalently chain rigidity, of the DNA can be expected to be important in relation to the molecular binding of DNA to Au, since the chain rigidity affects the entropy of association. This effect is clearly evidenced by the fact that oligomeric DNA in its much more rigid duplex form (the persistence length of dsDNA is an order of magnitude larger than that of ssDNA)<sup>67</sup> will adsorb strongly onto small Au NPs (14 nm) when single stranded DNA of a given sequence length will not. As with many polymers having a weakly attractive interaction with a substrate, ssDNA will undergo a transition from a non-adsorbed to an adsorbed state on Au with increasing chain length.<sup>62</sup> Importantly, DNA origami is a “woven” form of duplex DNA<sup>2</sup> so that the binding energy of AuNPs to DNA origami can be expected to be *greater* than that of the oligomeric ssDNA grafted onto the AuNP surface. Based on these trends in both experimental and computational studies of oligomeric DNA interacting with gold surfaces and AuNPs, we anticipate that the interactions between our AuNPs and the DNA origami will be attractive and strong and will influence the  $R_H$  of AuNP-origami constructs and we thus consider the effect of such an interaction in our modeling. Figures 7.a and 7.b show our predicted  $R_H$  results for these origami-NP complexes in the extreme cases of a null and attractive interaction, of order  $kT$ , between the AuNPs and origami, respectively. When there is no interaction, the origami remains relatively planar, and the  $R_H$  increases as more and larger particles are added. When an interaction is present, the overall trends of the experimental data are reproduced, with the same counter-intuitive decrease in  $R_H$  as more and larger AuNPs are attached. The particular values of  $R_H$  are sensitive to the exact strength of the attractive interaction in the simulation. The influence of the interaction strength on the origami deformation will be reported in a follow-up manuscript.

These results suggest that the DNA origami cannot be treated as an essentially planar platform, undergoing only modest conformational fluctuations that can accommodate NPs subject to purely geometrical constraints. The excluded volume interactions between the ssDNA on the AuNPs and the dsDNA of the origami and the interactions of the dsDNA of the origami with the AuNP surface can induce significant conformational changes. Because of the interplay of these many effects, the configuration of the origami-AuNP complexes can be strongly influenced by the size, number, and surface functionalization of the attached NPs. These factors should therefore be taken into account when designing, assembling, and purifying constructs.

### 3. Conclusions

We have demonstrated low-acceleration rate-zonal centrifugation to be a facile, high-yield separation method for various complex AuNP-DNA origami constructs, enabling > 90 % purities to be reached. This method is scalable and non-destructive, and capable of high resolution.

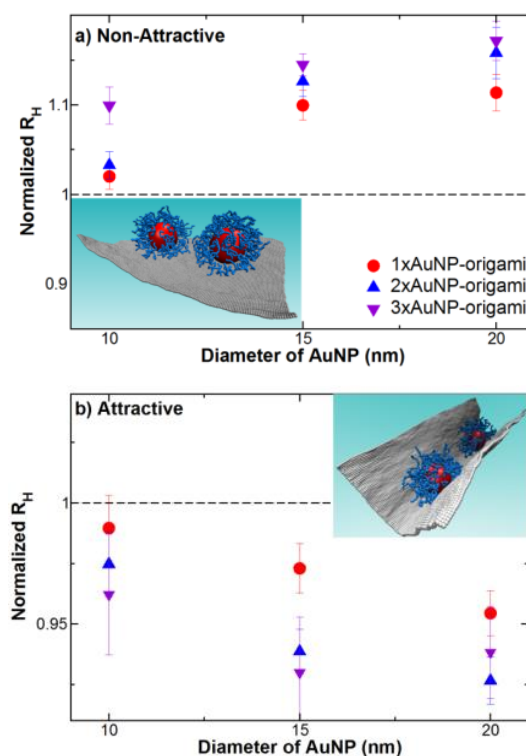


Fig. 7 Simulation of the normalized hydrodynamic radii of  $n$ AuNP-origami constructs assuming a) no interaction between the AuNP surface and the dsDNA of the origami, and b) the result of adding a WCA potential with energy scale  $\epsilon$ . Insets show how the conformation of the origami is affected by the interaction with the AuNPs.

It should be possible to further improve the separation resolution and the range of applicable particle sizes first by using nanoparticles with narrower size distributions<sup>26</sup> (Fig. S19) and then, as diffusion becomes the dominant cause of band broadening, by minimizing its effect through the combined use of high-viscosity media to reduce diffusion coefficients and higher spin-speeds to shorten separation times. The technique can be further enhanced as an effective purification method of NP-DNA nano-hybrid structures by incorporating a nanoparticle “handle”, which can only attach to well-folded structures, as the final part of an assembly, to permit separation of the target product. The ability to choose the mass of the “handle” enables the separation to be optimized. More design parameters are available: it is possible to distribute the desired mass in the form of multiple particles, and to choose their size and location to affect the conformation, and thus hydrodynamic radii of the constructs, to a greater or lesser extent. In addition, AuNPs enable direct visual detection of the target construct, greatly simplifying experimental extraction of the desired product. We expect that the high yields and purities obtained with this separation approach will open up the possibility of developing efficient, multi-step sequential reaction schemes for making more complex, hierarchical structures.

Finally, we have shown, through the comparison of hydrodynamic measurements and simulations of NP-origami constructs, that these systems exhibit complex conformational changes, caused by particle size-dependent interactions with ssDNA and dsDNA. By understanding the origins of these conformational changes, we can begin to devise ways of manipulating the particle-DNA interactions, e.g. via pH or salt

concentration, to add additional, dynamic functionality to these constructs.

## Acknowledgements

Dr. S. H. Ko acknowledges support under the Cooperative Research Agreement between the University of Maryland and the National Institute of Standards and Technology Center for Nanoscale Science and Technology, Award 70NANB10H193, through the University of Maryland. Dr. P. N. Patrone was supported by the National Institute of Standards and Technology American Recovery and Reinvestment Act Measurement Science and Engineering Fellowship Program Award No. 70NANB10H026 through the University of Maryland, with ancillary support from the NSF MRSEC under Grant No. DMR 05-20471, as well as the Condensed Matter Theory Center. Dr. P. N. Patrone's research was also supported by NSF DMS0847587 at the University of Maryland. The authors are grateful to Dr. V. A. Hackley and T. J. Cho for allowing us to use the DLS and helpful discussions. The authors thank Dr. J. Schumacher for help with SEM imaging and also thank Dr. J. Fagan for help with viscosity and density measurements. The authors also thank Dr. V. Szalai for many helpful discussions.

## Notes and references

<sup>a</sup> Center for Nanoscale Science and Technology, National Institute of Standards and Technology, Gaithersburg, MD 20899, United States.

<sup>b</sup> Maryland Nanocenter, University of Maryland, College Park, MD 20742, United States

<sup>c</sup> Material Science and Engineering Division, National Institute of Standards and Technology, Gaithersburg, Maryland 20899, United States

<sup>d</sup> Department of Physics, Institute for Research in Electronics and Applied Physics, and Condensed Matter Theory Center, University of Maryland, College Park, Maryland 20742-4111, United States

<sup>e</sup> Department of Physics, Wesleyan University, Middletown, Connecticut 06457, United States

<sup>§</sup> Current address: Center for Nanomaterials and Chemical Reactions, Institute for Basic Science (IBS), Daejeon 305-701, Korea

\* To whom correspondence should be addressed. E-mail: liddle@nist.gov.

Electronic Supplementary Information (ESI) available: See DOI: 10.1039/b000000x/

- N. R. Kallenbach, R. I. Ma and N. C. Seeman, *Nature*, 1983, **305**, 829.
- P. W. K. Rothmund, *Nature*, 2006, **440**, 297.
- B. Wei, M. Dai and P. Yin, *Nature*, 2012, **485**, 623.
- Y. Ke, L. L. Ong, W. M. Shih and P. Yin, *Science*, 2012, **338**, 1177.
- D. Han, S. Pal, Y. Yang, S. Jiang, J. Nangreave, Y. Liu and H. Yan, *Science*, 2013, **339**, 1412.
- A. Kuzuya and M. Komiyama, *Nanoscale*, 2010, **2**, 309.
- A. V. Pinheiro, D. Han, W. M. Shih and H. Yan, *Nature Nanotech.*, 2011, **6**, 763.
- V. Linko and H. Dietz, *Curr. Opin. Biotechnol.*, 2013, **24**, 1.
- R. Carlson, *Nat. Biotechnol.* 2009, **27**, 1091.
- J. J. Sobczak, T. G. Martin, T. Gerling and H. Dietz, *Science*, 2012, **338**, 1458.
- D. Smith, V. Schüller, C. Engst, J. Rädler and T. Liedl, *Nanomedicine*, 2013, **8**, 105.
- G. Bellot, M. A. McClintock, C. Lin and W. M. Shih, *Nature Methods*, 2011, **8**, 192.
- B. Ding, Z. Deng, H. Yan, S. Cabrini, R. N. Zuckermann and J. Bokor, *J. Am. Chem. Soc.*, 2010, **132**, 3248.
- X. Shen, A. Asenjo-Garcia, Q. Liu, Q. Jiang, F. J. G. Abajo, N. Liu and B. Ding, *Nano Lett.*, 2013, **13**, 2128.
- W. Mächtle and L. Börger, in *Analytical Ultracentrifugation of Polymers and Nanoparticles*, Springer-Verlag, Berlin, 2006.
- J. Lebowitz, M. S. Lewis and P. Schuck, *Prot. Sci.* 2002, **11**, 2067.
- G. Cadisch, M. Espana, R. Causey, M. Richter, E. Shaw, J. A. W. Morgan, C. Rahn and G. D. Bending, *Rapid Commun. Mass Spectrom.*, 2005, **19**, 1424.
- C. Lin, S. D. Perrault, M. Kwak, F. Graf and W. M. Shih, *Nucleic Acids Res.*, 2012, **40**, 1.
- L. Bai, X. Ma, J. Liu, X. Sun, D. Zhao and D. G. Evans, *J. Am. Chem. Soc.*, 2010, **132**, 2333.
- X. Ma, Y. Kuang, L. Bai, Z. Chang, F. Wang, X. Sun and D. G. Evans, *ACS Nano*, 2011, **5**, 3242.
- O. Akbulut, C. R. Mace, R. V. Martinez, A. A. Kumar, Z. Nie, M. R. Patton and G. M. Whitesides, *Nano Lett.* 2012, **12**, 4060.
- M. S. Arnold, A. A. Green, J. F. Hulvat, S. I. Stupp and M. C. Hersam, *Nature Nanotech.*, 2006, **1**, 60.
- J. A. Fagan, M. L. Becker, J. Chun and E. K. Hobbie, *Adv. Mater.*, 2008, **20**, 1609.
- X. Sun, D. Luo, J. Liu and D. G. Evans, *ACS Nano*, 2010, **4**, 3381.
- J. A. Fagan, M. Zheng, V. Rastogi, J. R. Simpson, C. Y. Khrpin, C. A. Silvera Batista and A. R. Hight Walker, *ACS Nano*, 2013, **7**, 3373.
- A. Fritsch, in *Preparative Density Gradient Centrifugations*, Beckman, Genève, 1975.
- D. Velegol, S. Shori and C. E. Snyder, *Ind. Eng. Chem. Res.*, 2009, **48**, 2414.
- T. Torring, N. V. Voigt, J. Nangreave, H. Yan and K. V. Kothelf, *Chem. Soc. Rev.* 2011, **40**, 5636.
- G. P. Acuna, F. M. Möller, P. Holzmeister, S. Beater, B. Lalkens and P. Tinnefeld, *Science*, 2012, **338**, 506.
- A. Kuzyk, R. Schreiber, Z. Fan, G. Pardatscher, E. Roller, A. Hogege, F. C. Simmel, A. O. Govorov and T. Liedl, *Nature*, 2012, **483**, 311.
- X. Shen, C. Song, J. Wang, D. Shi, Z. Wang, N. Liu and B. Ding, *J. Am. Chem. Soc.*, 2012, **134**, 146.
- Z. Zhao, E. L. Jacovetty, Y. Liu and H. Yan, *Angew. Chem. Int. Ed.*, 2011, **50**, 1.
- B. Ding, Z. Deng, H. Yan, S. Cabrini, R. N. Zuckermann and J. Bokor, *J. Am. Chem. Soc.*, 2010, **132**, 3248.
- Y. H. Roh, R. C. H. Ruiz, S. Peng, J. B. Lee and D. Luo, *Chem. Soc. Rev.* 2011, **40**, 5730.
- M. Endo, Y. Yang, T. Emura, K. HiDaka and H. Sugiyama, *Chem. Commun.* 2011, **47**, 10743.
- X. Shen, A. Asenjo-Garcia, Q. Liu, Q. Jiang, F. J. G. Abajo, N. Liu and B. Ding, *Nano Lett.*, 2013, **13**, 2128.
- A. M. Hung, C. M. Micheel, L. D. Bozano, L. W. Osterbur, G. M. Wallraff and J. N. Cha, *Nature Nanotech.*, 2010, **5**, 121-126.
- D. Velegol, S. Shori and C. E. Snyder, *Ind. Eng. Chem. Res.*, 2009, **48**, 2414.
- X. Pang, L. Zhao, W. Han, X. Xi and Z. Lin, *Nature Nanotech.*, 2013, **8**, 426.

40. The width of the band due to diffusion and the initial band width is calculated by assuming diffusion occurs out of a slab of fixed initial concentration. The diffusion coefficient,  $D$ , can be calculated using the following equation;  $D = kT/6\pi\eta R_H$ , where  $k$  is Boltzmann's constant,  $T$  is temperature,  $\eta$  is the viscosity and  $R_H$  the hydrodynamic radius. The calculated nominal  $D$  of AuNP-DNA origami constructs is  $3 \times 10^{-12} \text{ m}^2/\text{s}$ , using  $R_H = 35 \text{ nm}$  and  $\eta = 2 \text{ mPa}\cdot\text{s}$  as an initial value of the viscosity. To estimate a worst-case broadening, we assume a maximum centrifugation time of 270 min., and a band that is 0.5 mm thick upon loading. At the end of the centrifugation, this will have assumed a profile with a half-width, half-maximum of approximately 0.4 mm ( $\sigma$  of the corresponding Gaussian is approximately 0.3 mm). This can be compared with typical band  $\sigma$  values of 1 mm. Assuming a root sum of squares addition, the effect of diffusion and the initial band width account for only about 5 % of the observed broadening.
41. If we assume that pipetting can be used to extract all the material within  $\pm \sigma$  of the band maximum, then a purity of 90 % can be achieved as long as the maximum of next band (having the same spread) is at least  $2.5 \sigma$  away.
42. M. L. Mansfield, J. F. Douglas and E. J. Garboczi, *Phys. Rev. E*, 2001, **64**, 061401.
43. M. L. Mansfield, J. F. Douglas, S. Irfan and E. H. Kang, *Macromolecules*, 2007, **40**, 2575.
44. <http://www.stevens.edu/zeno/>
45. J. F. Douglas, H. Zhou and J. B. Hubbard, *Phys. Rev. E*, 1994, **49**, 5319.
46. O. Padovan-Merhar F. Vargas-Lara and F. Starr, *J. Chem. Phys.*, 2011, **134**, 244701.
47. S. Knauert, J. Douglas and F. Starr, *Macromolecules*, 2010, **43**, 3438.
48. K. Kremer, G. S. Grest, *J. Chem. Phys.*, 1990, **92**, 5057.
49. M. L. Mansfield, J. F. Douglas, *Macromolecules*, 2008, **41**, 5412.
50. S. Knauert, J. Douglas, F. Starr, *Macromolecules*, 2010, **43**, 3438.
51. L. M. Demers, C. A. Mirkin, R. C. Mucic, R. A. Reynolds, R. L. Letsinger, R. Elghanian, and G. Viswanadham, *Anal. Chem.* 2000, **72**, 5535.
52. H. D. Hill, J. E. Millstone, M. J. Banholzer, and C. A. Mirkin, *ACS Nano*, 2009, **3**, 418.
53. S. J. Hurst, A. K. R. Lytton-Jean, and C. A. Mirkin, *Anal. Chem.* 2006, **78**, 8313.
54. J. Turkevich, *Gold Bull.*, 1985, **18**, 125.
55. J. J. Storhoff, R. Elghanian, C. A. Mirkin and R. L. Letsinger, *Langmuir*, 2002, **18**, 6666.
56. R. Schreiber, J. Do, E. Roller, T. Zhang, V. J. Schüller, P. C. Nickels, J. Feldmann and T. Liedl, *Nature Nanotech.*, 2014, **9**, 74.
57. X. Zhang, T. Gouriye, K. Göeken, M. R. Servos, R. Gill and J. Liu, *J. Phys. Chem. C*, 2013, **117**, 15677.
58. J. Liu, *PhysChemChem Phys.*, 2012, **14**, 10485.
59. P. Sandström and B. Åkerman, *Langmuir*, 2004, **20**, 4182.
60. H. Kimura-Suda, D. Y. Petrovykh, M. J. Tarlov and L. J. Whitman, *J. Am. Chem. Soc.* 2003, **125**, 9014.42. J. Turkevich, *Gold Bull.*, 1985, **18**, 125.
61. T. Herne and M. Tarlov, *JACS* 1997, **119**, 8916 (1997)
62. L. Gearheart H. Ploehn, C. Murphy, *J. Phys. Chem. B*, 2001, **105**, 12609
63. M. Berg, R. Coleman and C. Murphy, *Phys. Chem. Chem. Phys.* 2008, **10**, 1229
64. S. Lacerda, M. Park, C. Meuse, D. Pristiniski, M. Becker, A. Karim, J. F. Douglas, *ACS Nano* 2010, **4**, 365
65. J. Feng, R. Pandey, R. Berry, B. Farmer, R. Naik, H. Heinz, *Soft Matter* 2011, **7**, 2113
66. C. Goodman, N. Chari, G. Han, R. Hong, P. Gosh, V. Rotello., *Chem. Biol. Drug Design* 2006, **67**, 297
67. B. Tinland, A. Pluen, J. Sturm, J. Weill, *Macromolecules*, 1997, **30** (19), pp 5763–5765

## Supplementary information

for

### High-speed, high-purity separation of gold nanoparticle-DNA origami constructs using centrifugation

Seung Hyeon Ko, Fernando Vargas-Lara, Paul N. Patrone, Samuel M. Stavis, Francis W. Starr, Jack F. Douglas, and J. Alexander Liddle\*

#### Experimental

**Disclaimer:** Certain commercial equipment, instruments, or materials are identified in order to specify the experimental procedure adequately. Such identification is not intended to imply recommendation or endorsement by the National Institute of Standards and Technology, nor is it intended to imply that the materials or equipment identified are necessarily the best available for the purpose.

**Materials:** We purchased single strand M13mp18 and thiol conjugated single-stranded DNA strands commercially. We purchased all unmodified and poly-A labeled DNA staple strands commercially, and used them without further purification. We purchased colloidal solutions of AuNPs and all other chemicals commercially.  $1\times$  TAE/Mg<sup>2+</sup> buffer contains 40 mmol L<sup>-1</sup> (mM) tris(hydroxymethyl)aminomethane (tris), 20 mmol L<sup>-1</sup> (mM) acetic acid, 2 mmol L<sup>-1</sup> (mM) ethylenediaminetetraaceticacid (EDTA), and 12.5 mmol L<sup>-1</sup> (mM) magnesium acetate, pH 8.0 and  $0.5\times$  TBE buffer has 45 mmol L<sup>-1</sup> (mM) tris(hydroxymethyl)aminomethane (tris), 45 mmol L<sup>-1</sup> (mM) Boric acid, and 1 mmol L<sup>-1</sup> (mM) ethylenediaminetetraaceticacid (EDTA).

**Self-assembly of DNA origami:** We assembled rectangular DNA origami according to the method of Rothmund.<sup>1</sup> We mixed a long single strand of M13mp18 and staple strands at a molar ratio of 1 to 5 in  $1\times$  TAE/Mg<sup>2+</sup> buffer and slowly annealed the strands at 1 °C min<sup>-1</sup>

---

\* E-mail: liddle@nist.gov

from 95 °C to room temperature using a DNA thermal cycler. We removed excess staple strands by washing four to five times with 1× TAE/Mg<sup>2+</sup> buffer (400 μL) in a “100 000 molecular weight cut-off (MWCO) filter” (100 kDa MWCO) microcentrifuge filter at an acceleration of 600 rad s<sup>-1</sup> (5 730 rpm, 34 355 m s<sup>-2</sup>, 3 500 × g) for 2 min. We omitted staple strands on vertical edges to avoid stacking of origami along vertical edges.

**Functionalization of AuNP with ssDNA:** We stabilized AuNPs by adsorption of bis(parasulfonatophenyl) phenylphosphine dihydrate dipotassium salt (phosphine salt). Typically, we added 10 mg of phosphine salt to 50 mL of AuNP solution, shaking the mixture overnight at room temperature. We then precipitated the AuNPs by adding sodium chloride until the color turned bluish purple. After centrifugation at 850 rad s<sup>-1</sup> (68 670 m s<sup>-2</sup>, 7 000 × g) for several minutes, we removed the supernatant with a pipette, and re-dispersed the AuNP precipitate in 2.5 mmol L<sup>-1</sup> (mM) phosphine solution. We mixed dithiolated DNA and phosphine-protected AuNPs at various molar ratios, which depended on the size of AuNPs, and pre-incubated for an hour. We added solutions of TBE buffer (10×), SDS (0.01%) and NaCl (1 mol L<sup>-1</sup>) to pre-incubated AuNPs and ssDNA and brought the final concentrations of TBE, SDS, and NaCl to 0.5×, 0.01%, and 0.05 mol L<sup>-1</sup> (M), respectively. We left the solution of AuNP/DNA in buffer for two hours at room temperature. We slowly increased the NaCl concentration of the solution to 0.5 mol L<sup>-1</sup> (M) by sequential additions of 0.5× TBE buffer (0.01% SDS)/1 mol L<sup>-1</sup> (M) NaCl and incubated the mixture for 24 h at room temperature. We purified conjugates of ssDNA-AuNP by spin column in a microcentrifuge.

**Preparation of AuNP-DNA Origami Constructs:** We mixed DNA origami solution with ssDNA functionalized AuNP solution at 1.3× to 2× molar ratio to the binding locations on an origami and slowly annealed the solution from 37 °C to room temperature using a DNA thermal cycler.

***Centrifugation of AuNP-DNA Origami Constructs:*** We used a medium of nine-layers of different concentrations of iodixanol (10%, 15%, ..., 50%) for centrifugation of AuNP-DNA origami constructs. We denote the different constructs as  $n$ AuNP-origami, where  $n$  is the number of AuNP bound to an origami. We prepared iodixanol solutions of different concentrations as follows: we first diluted commercial (Optiprep™, Sigma-Aldrich), 60% (w/v) iodixanol in water by  $6\times$  TAE/Mg<sup>2+</sup> (*i.e.*, 6 times more concentrated than  $1\times$  TAE/Mg<sup>2+</sup>) to 50% iodixanol in  $1\times$  TAE/Mg<sup>2+</sup>. We prepared all other solutions by sequential dilution of 50% iodixanol in  $1\times$  TAE/Mg<sup>2+</sup> with  $1\times$  TAE/Mg<sup>2+</sup>. We prepared the nine-layer density gradient medium in a centrifuge tube a day prior to centrifugation. We loaded the sample solution on top of the density gradient in the centrifuge tube, and then centrifuged it at various speeds (in an Eppendorf Microcentrifuge, Model 5417R) depending on the size of AuNP to get separation of bands. We used a swing bucket rotor (Eppendorf A-8-11) in all experiments and the centrifuge temperature was set to 20 °C with an uncertainty, as specified by the vendor, of  $\pm 2$  °C. We recovered each band from the medium after sedimentation of the constructs was complete by pipetting. We buffer-exchanged the iodixanol medium for  $1\times$  TAE/Mg<sup>2+</sup> buffer by spin column.

***Scanning Electron Microscope (SEM) Characterization of AuNP-DNA Origami Constructs:*** A silicon wafer was treated with oxygen plasma before SEM imaging. We loaded a solution of AuNP-DNA origami (5  $\mu$ L) onto an oxygen plasma-treated Si wafer, allowed it to rest for a minute, and quickly washed the wafer with water. We imaged the sample by SEM with an incident electron energy of 1.0 kV.

***Dynamic Light Scattering (DLS) Measurements of AuNP-DNA Origami Constructs:*** We performed dynamic light scattering measurements using non-invasive backscatter optics with 45  $\mu$ L samples in low-volume quartz batch cuvette. We set the temperature to 20 °C.

## Results and Analysis

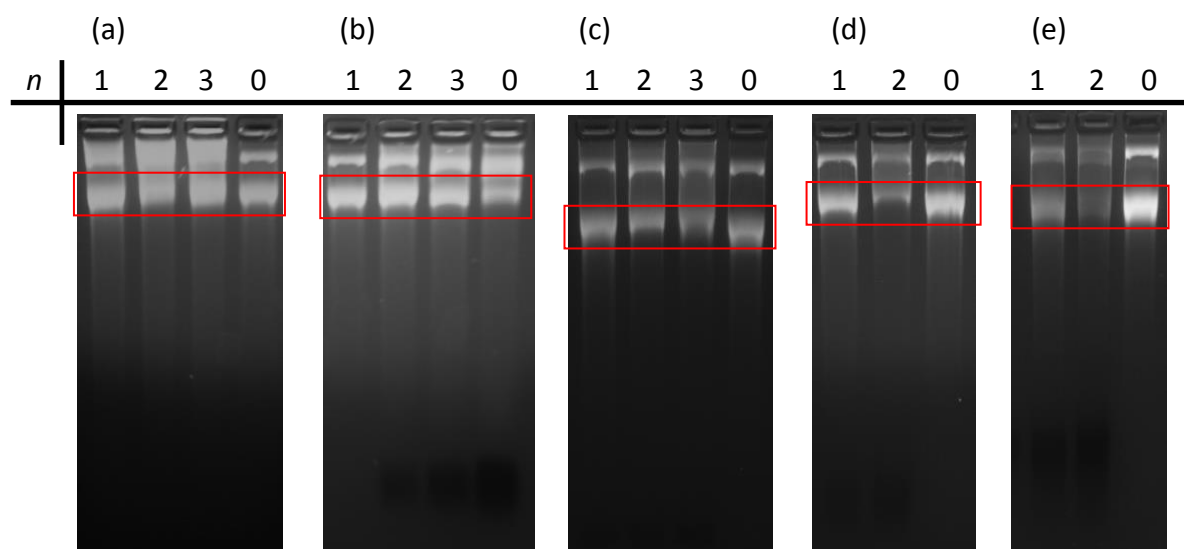


**Figure S1.** 1.5% agarose gel of (a) 5 nm AuNP-origami, (b) 10 nm AuNP-origami, (c) 15 nm AuNP-origami, (d) 20nm AuNP-origami, and (e) 30 nm AuNP-origami conjugates. The gels were pre-stained by ethidium bromide to visualize the band of the products.  $n$  represents the desired number of AuNP attached to DNA origami. The bands of desired product are highlighted by red boxes. The slower moving bands are probably cross-linked origami, as indicated by a previous study.<sup>2</sup>

**Table S1.** Dynamic viscosity and density of centrifugation media at  $20.0 \pm 0.1$  °C (average  $\pm$  limit of uncertainty)

Notes	Volume fraction of iodixanol (%)	Dynamic viscosity (mPa s)	Density (g cm <sup>-3</sup> )
in 1× TAE/Mg <sup>2+</sup> buffer	0	1.02	1.000
"	5	1.14	1.027
"	10	1.31	1.054
"	15	1.49	1.079
"	20	1.75	1.107
"	25	2.10	1.134
"	30	2.54	1.160
"	35	3.21	1.188
"	40	4.11	1.214
"	45	5.42	1.241
"	50	6.97	1.262
in water (OptiPrep™)	60	14.33	1.320

The limits of uncertainty on dynamic viscosity and density are  $\pm 0.01$  mPa s and  $\pm 0.001$  g cm<sup>-3</sup> respectively

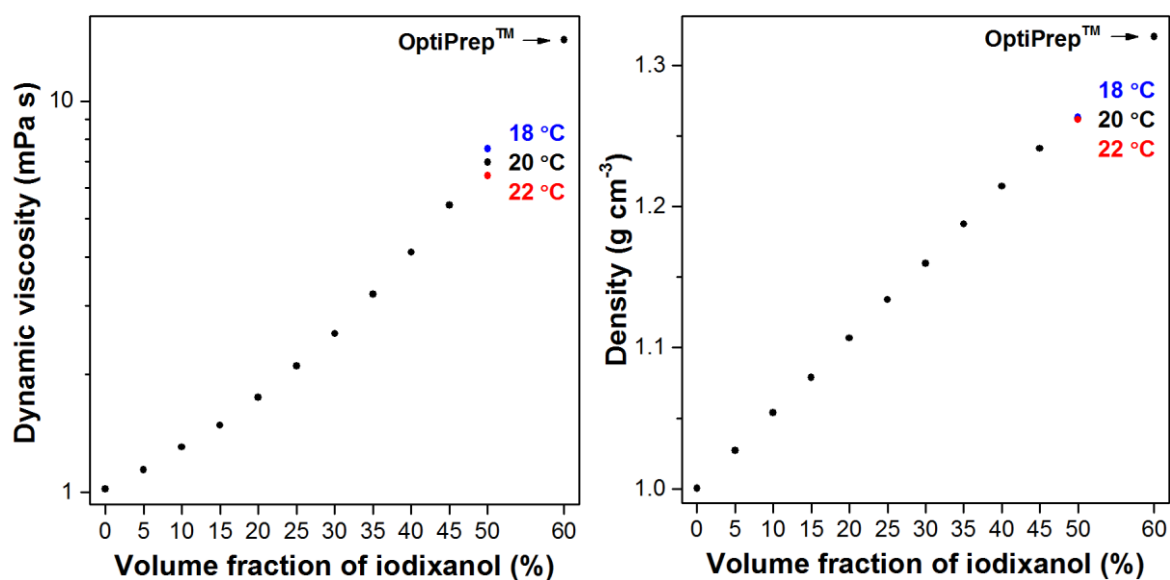


**Figure S2.** Dynamic viscosity and density increase as a function of volume fraction of iodixanol in water. The limits of uncertainty for all variables are smaller than the data points. A 2 °C variation in temperature around 20 °C, corresponds to the uncertainty in medium temperature during centrifugation, and results in an  $\approx 8\%$  variation in dynamic viscosity.

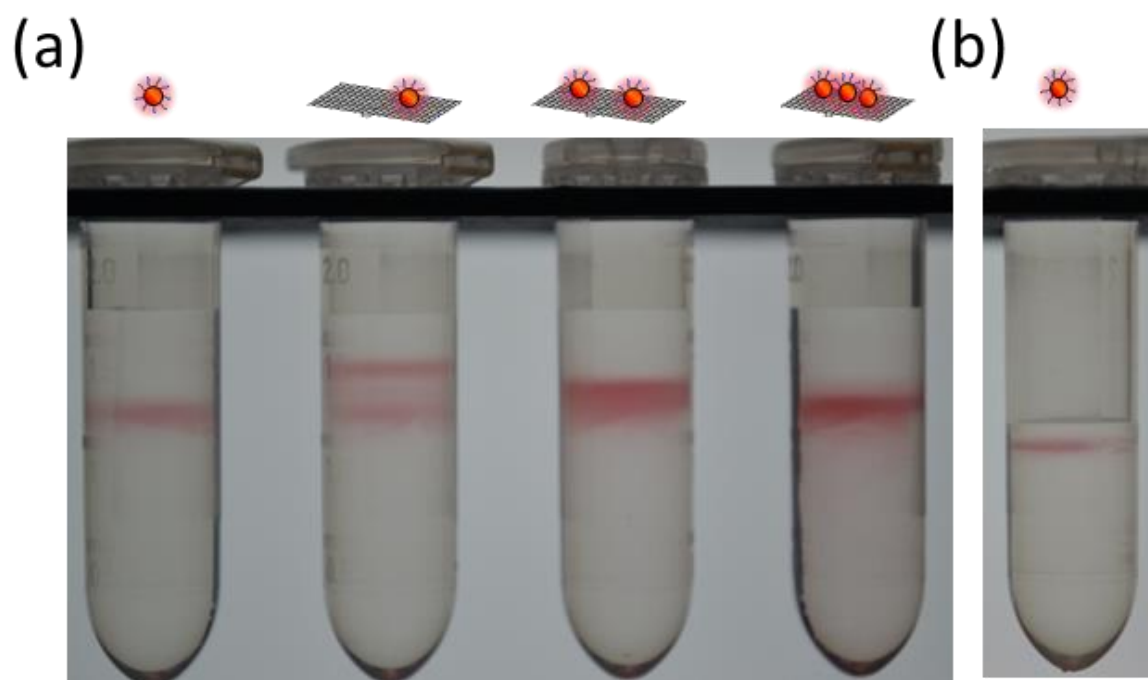


**Figure S3.** Separation of 10 nm AuNP constructs by centrifugation (a) after 240 min in 50% glycerol. Different constructs (2AuNP-origami and 3AuNP-origami) were not separated from free AuNPs. (b) 10 nm AuNP after 60 min of centrifugation in 50 % iodixanol. The layer of AuNP was not stable during centrifugation. The centrifugation speed was  $850 \text{ rad s}^{-1}$  (8 100 rpm,  $68\,600 \text{ m s}^{-2}$ ,  $7\,000 \times g$ ) for both.

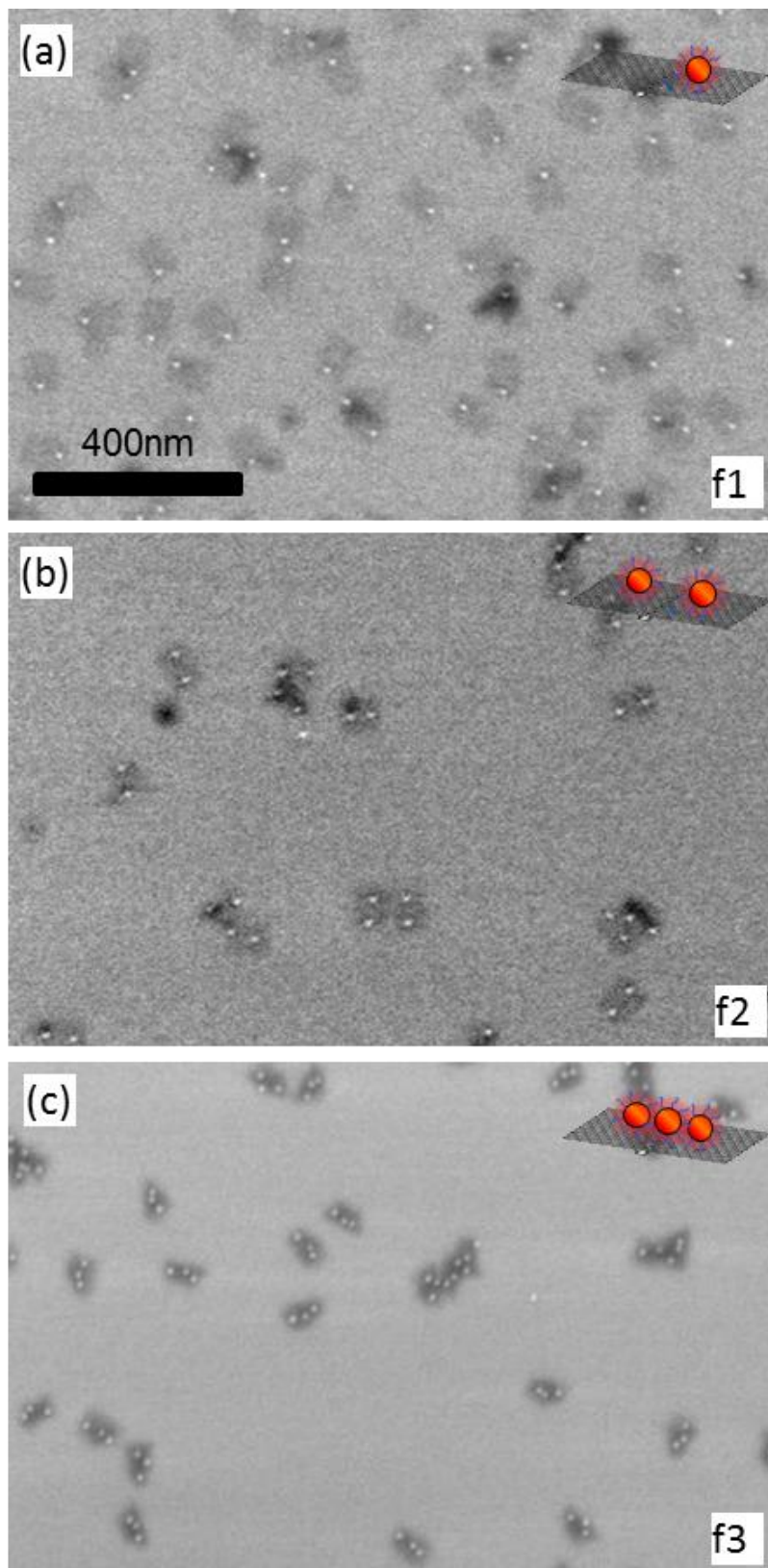


**Figure S4.** Typical SEM images of different fractions of  $n=10$  nm AuNP-origami conjugates as labeled in Figure 2 (a) after centrifuge purification. The fraction f1 is  $(96.1 \pm 0.5)\%$  1AuNP-origami, f2 is  $(94.6 \pm 1.0)\%$  2AuNP-origami, and f3 is  $(92.9 \pm 1.3)\%$  3AuNP-origami.

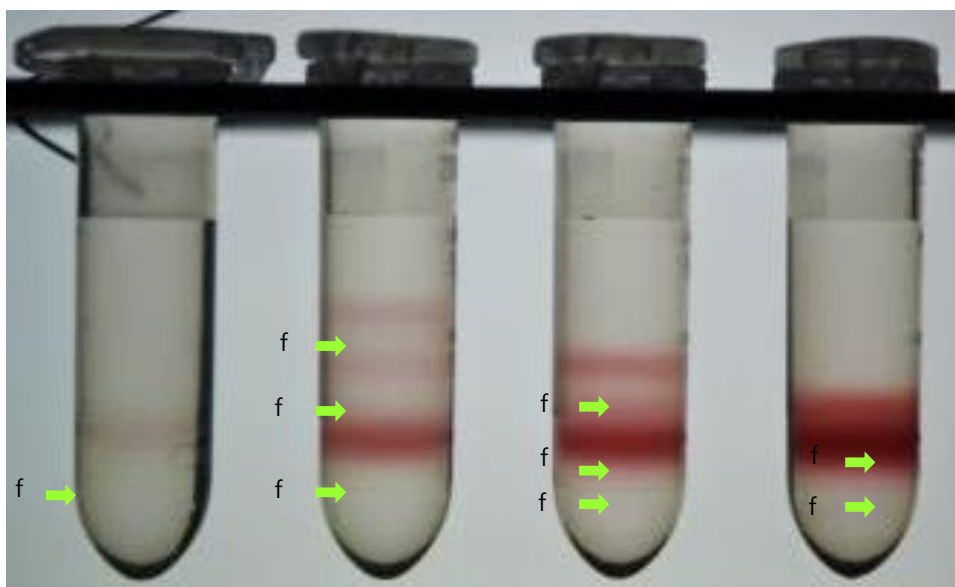


**Figure S5.** Separation of  $n10$  nm AuNP constructs by centrifugation. Different fractions of  $n10$  nm AuNP-origami constructs are labeled the same as Figure 2a. The centrifugation speed was  $850 \text{ rad s}^{-1}$  ( $8\ 100 \text{ rpm}$ ,  $68\ 600 \text{ m}\cdot\text{s}^{-2}$ ,  $7\ 000 \times g$ ).

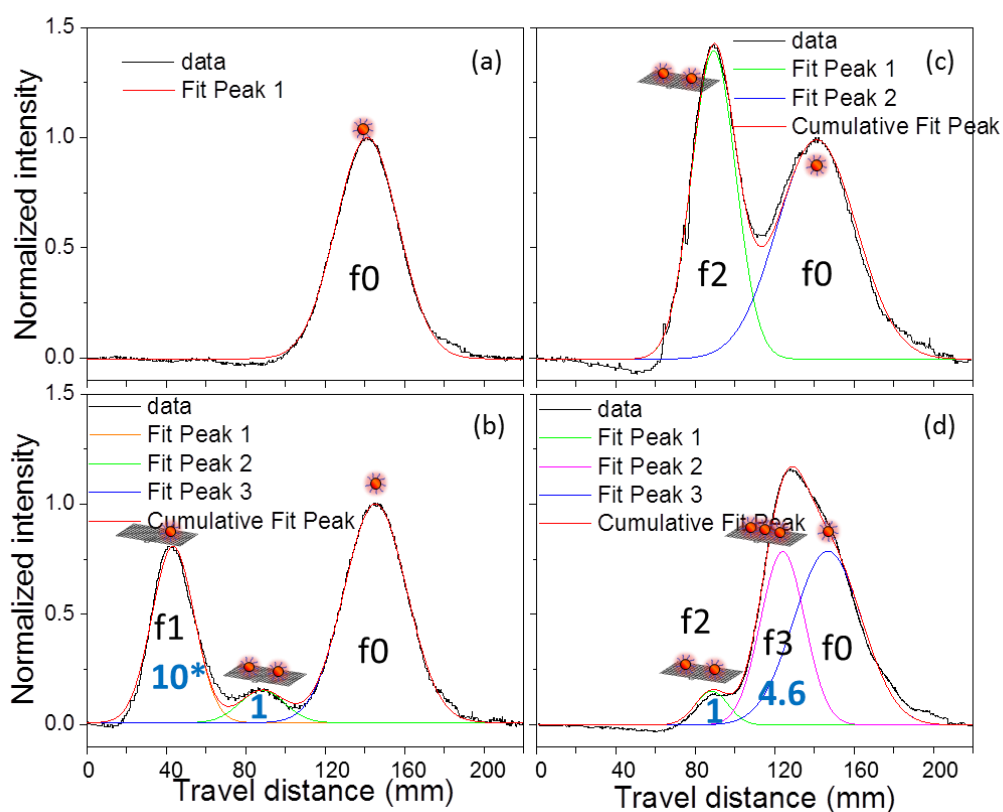


**Figure S6.** Centrifugrams of  $n10$  nm AuNP-origami conjugates of each tube from the left to the right ((a) to (d)) in Figure 2 (a). Each band has been labeled as Figure 2 and fitted by a Gaussian function. The blue numbers in (b) and (d) are the values of the calculated area of the corresponding peak divided by the number of AuNP. These and the following Gaussian fits are not quantitative, due to variability in background illumination intensity, but rather provide a qualitative estimate of the relative fractions of the various constructs present.

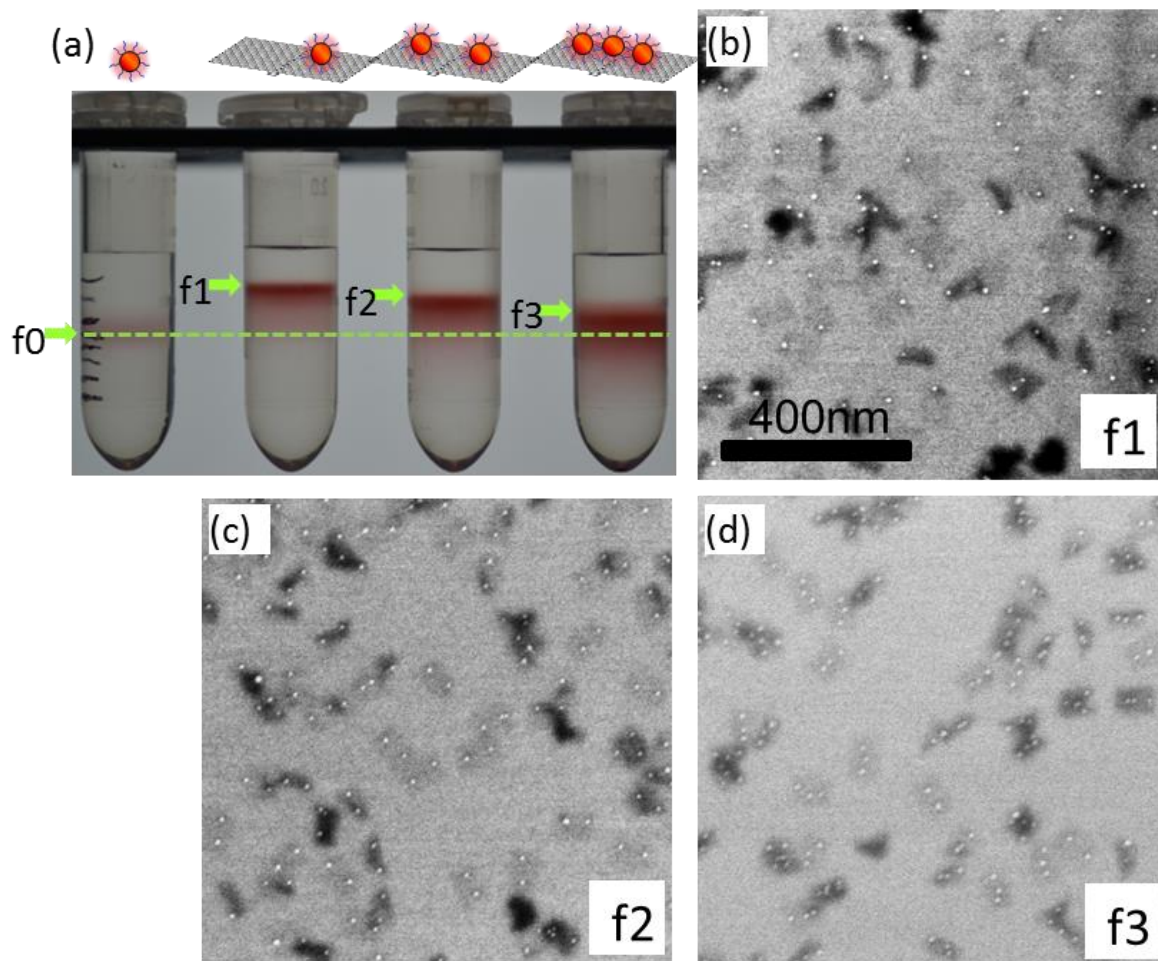


**Figure S7.** (a) Photograph of the centrifuge tubes containing different conjugates of 5 nm AuNP-DNA origami after spinning for 150 min at  $1100 \text{ rad s}^{-1}$  (10 500 rpm,  $114\,660 \text{ m s}^{-2}$ ,  $11\,700 \times g$ ). (b)-(d) SEM images of different fractions of AuNP-origami conjugates as labeled in (a). The yields are  $\approx 100\%$ ; within our measurement uncertainty.

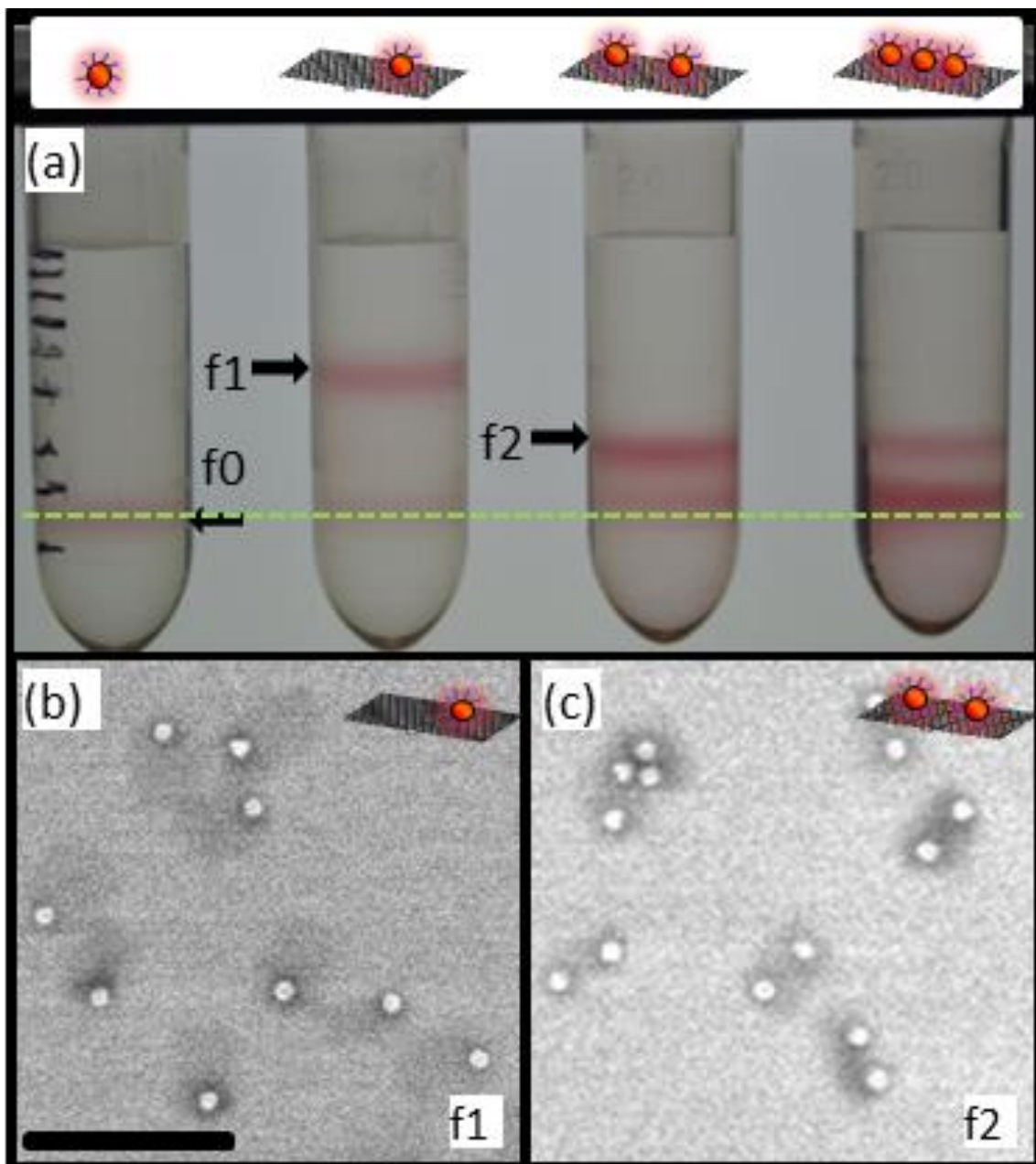


**Figure S8.** Separation of  $n15$  nm AuNP-DNA origami. (a) Photograph of centrifuge tubes containing different constructs after spinning for 3 h at  $681 \text{ rad s}^{-1}$  (6 500 rpm,  $44\,100 \text{ m s}^{-2}$ ,  $4500 \times g$ ). (b)-(d) Typical SEM images of different fractions of AuNP-origami constructs as labeled in (a). Schematics of the target product are shown for each tube. The fraction labeled f0 corresponds to free AuNPs. The SEM scale bar is 200 nm. Each construct ( $n = 1$  and 2) is clearly separated, based on the differences in sedimentation coefficients. Analysis of the SEM micrographs shows that the slowest fraction, f1, is  $(96.9 \pm 1.1)\%$  1AuNP-origami and the fraction f2 is  $(95.8 \pm 1.3)\%$  2AuNP-origami.

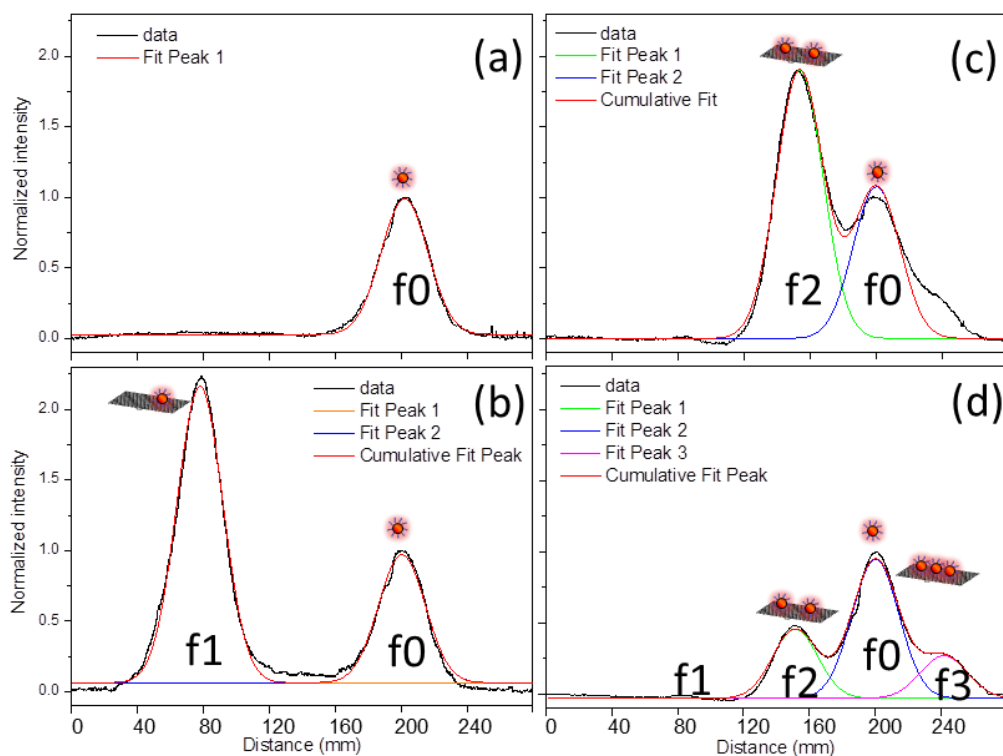


**Figure S9.** Centrifugation profiles of  $n15$  nm AuNP-origami conjugates of each tube from the left to the right ((a) to (d)) in Figure 3 (a). Each band has been labeled as in Figure S7 and fitted by a Gaussian function.

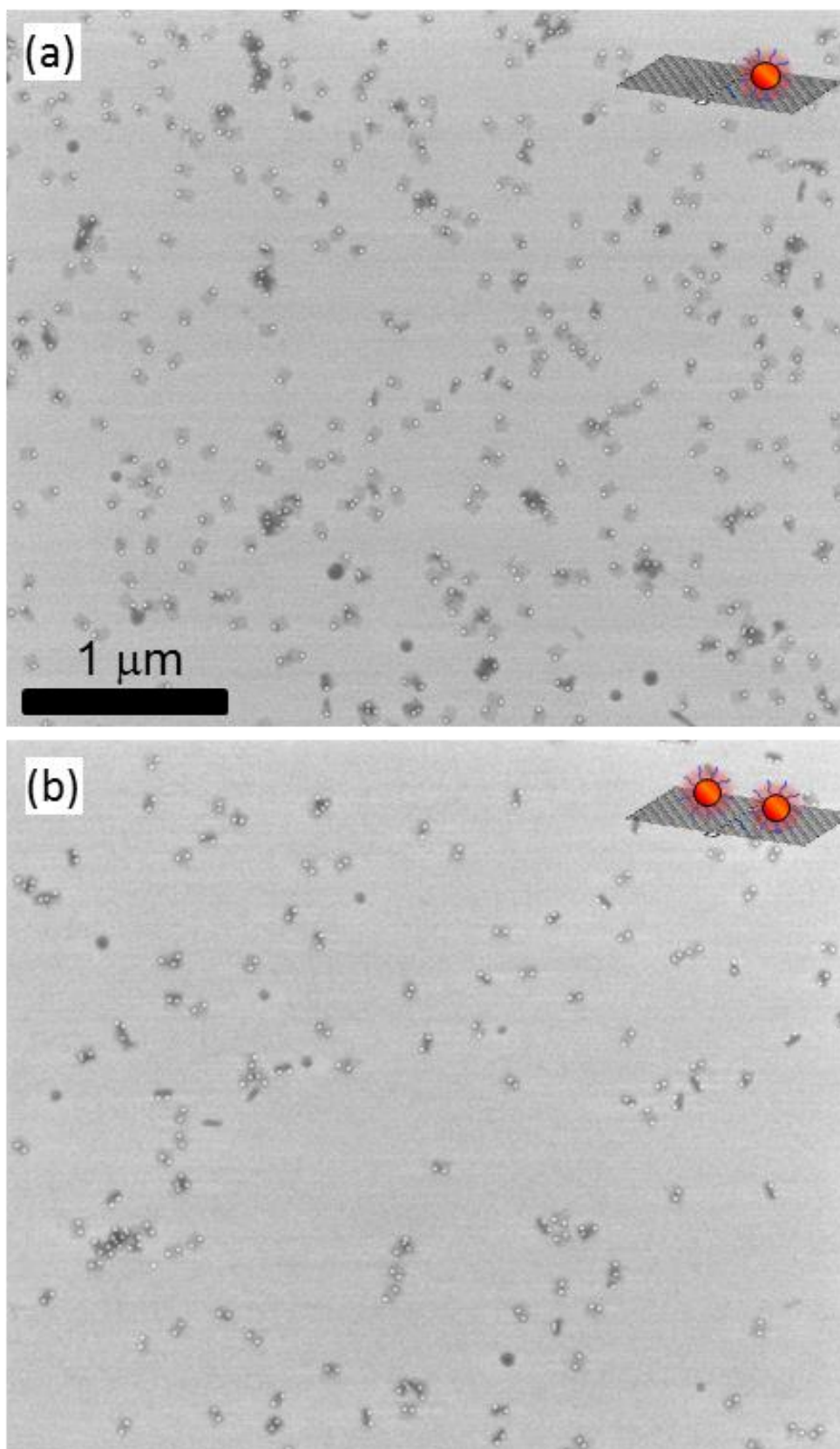


**Figure S10.** Typical SEM images of different fractions of  $n15$  nm AuNP-origami conjugates after centrifuge purification. Each construct ( $n = 1$  and  $2$ ) is clearly separated, based on the differences in sedimentation coefficients. Analysis of the SEM micrographs shows that the slowest fraction f1 contains  $(96.9 \pm 1.1)\%$  1AuNP-origami and f2 is  $(95.8 \pm 1.3)\%$  2AuNP-origami.

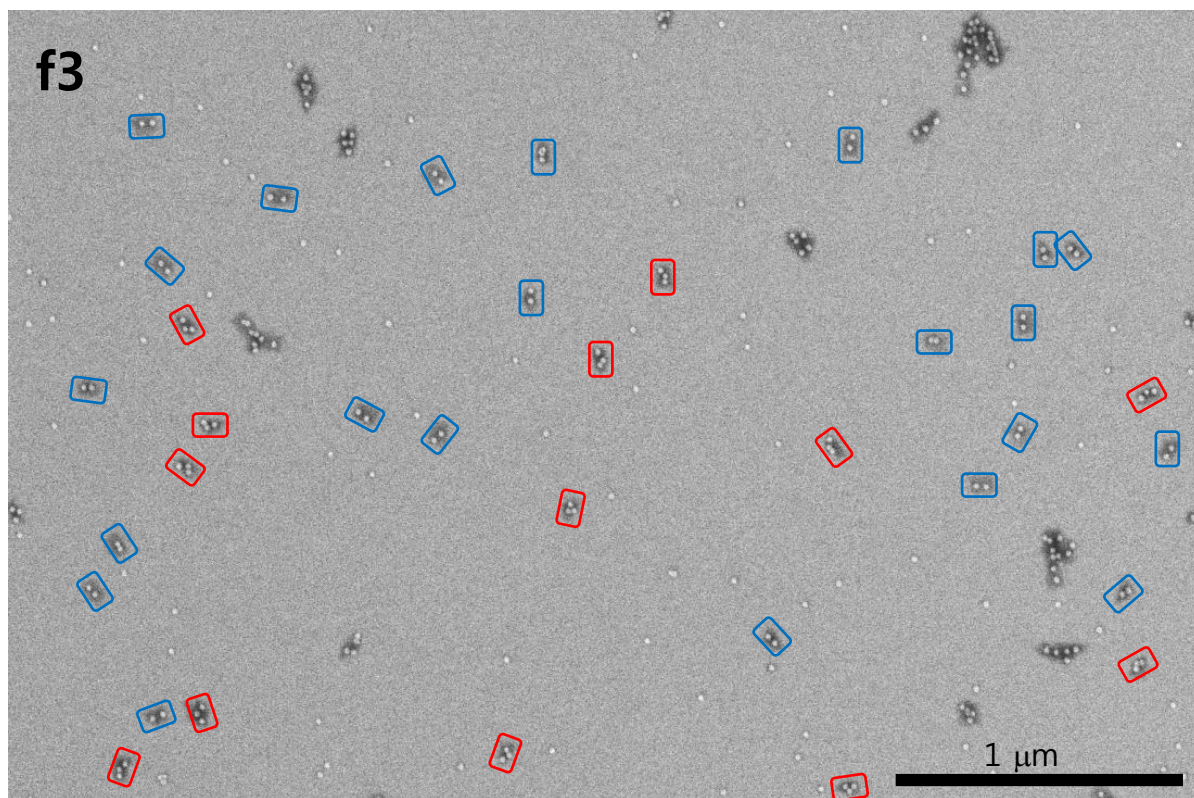


**Figure S11.** SEM images of the band f3 (Figure S7) separated from the centrifugation tube targeting 15 nm 3AuNP-origami. A blue rectangle highlights 2AuNP-origami and a red rectangle shows 3AuNP-origami. The fractions of 2AuNP-origami and 3AuNP-origami are  $(62 \pm 8)\%$  and  $(37 \pm 8)\%$ , respectively.

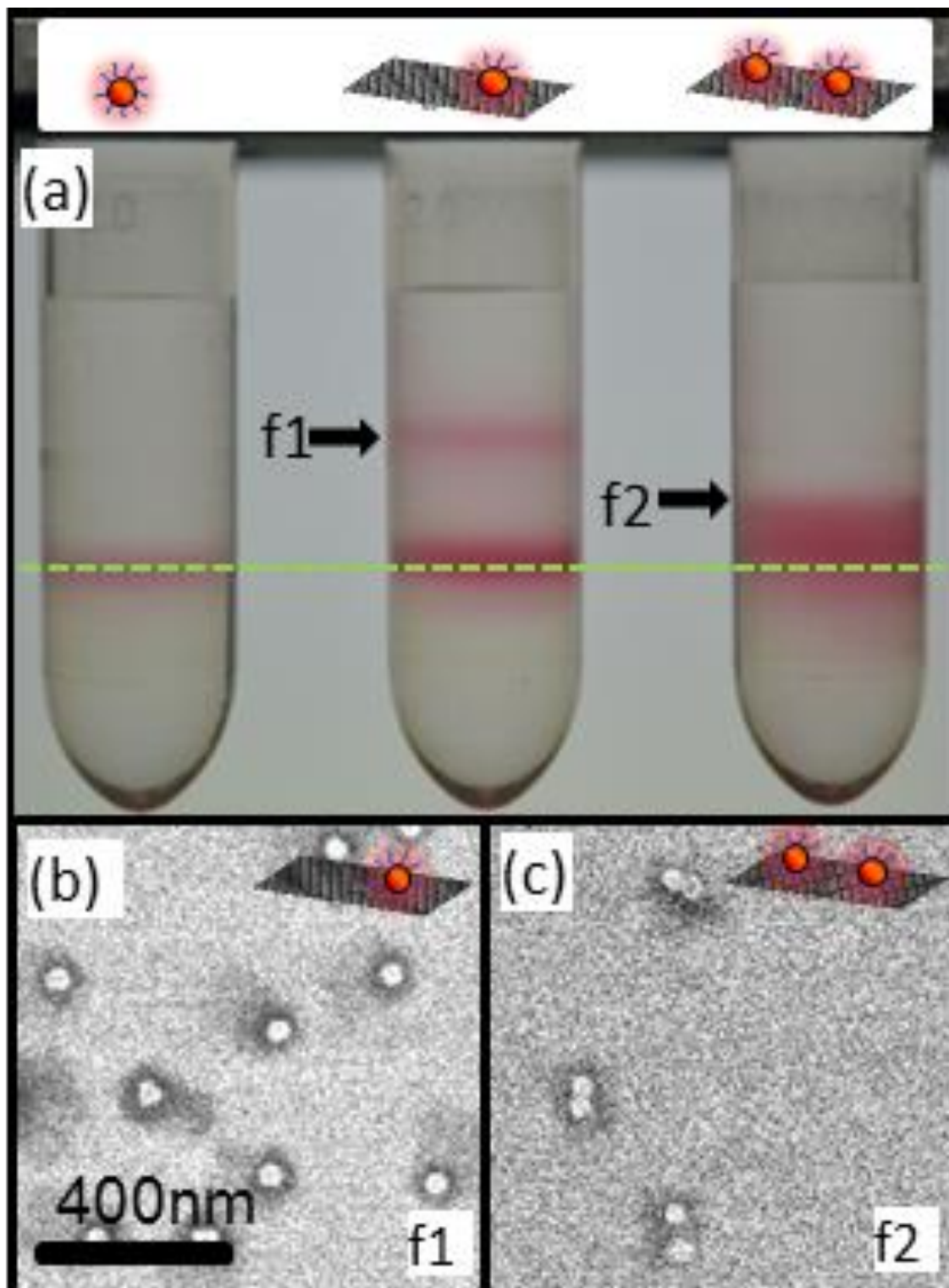


**Figure S12.** Separation of 20 nm AuNP-DNA origami. (a) Photograph of centrifuge tubes containing different constructs after spinning for 2 hours at  $508 \text{ rad s}^{-1}$  (4 850 rpm,  $24\,500 \text{ m s}^{-2}$ ,  $2\,500 \times g$ ). (b)-(d) Typical SEM images of different fractions of AuNP-origami constructs as labeled in (a). Schematics of the target product are shown for each tube. The SEM scale bar is 200 nm.

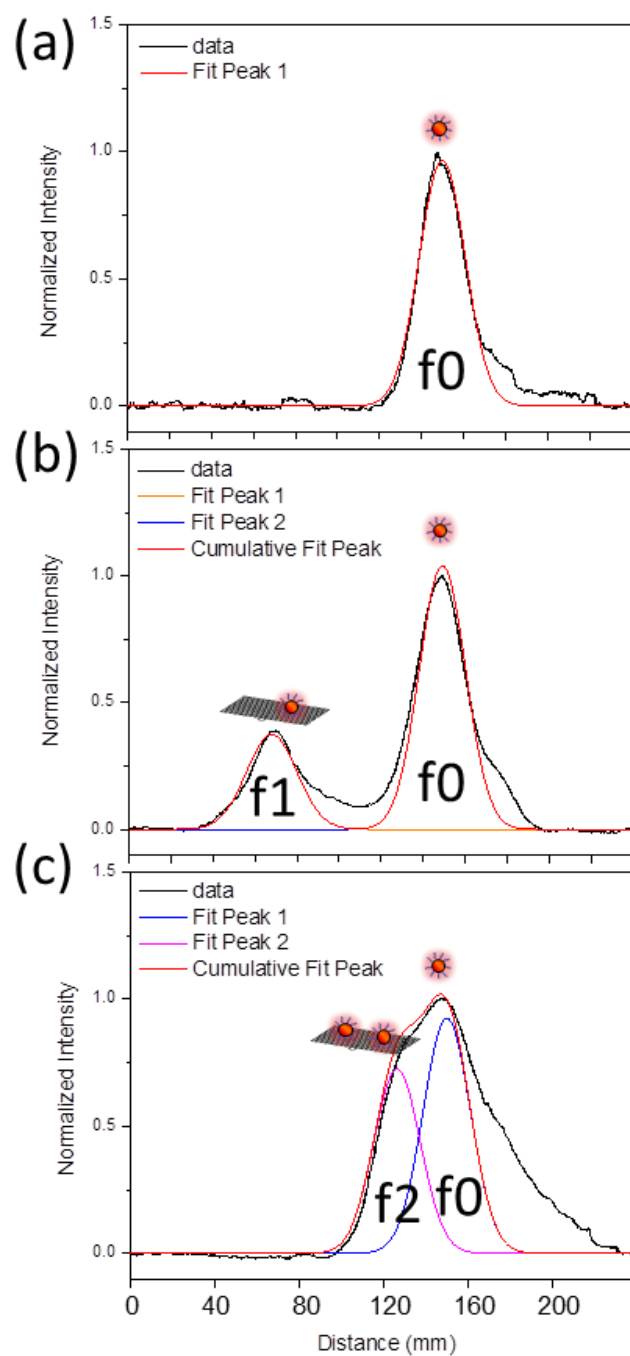


**Figure S13.** Centrifugam of  $n20$  nm AuNP-origami conjugates of each tube from the left to the right ((a) to (c)) in Figure S11 (a). Each band has been labeled as Figure S11 and fitted by a Gaussian function.

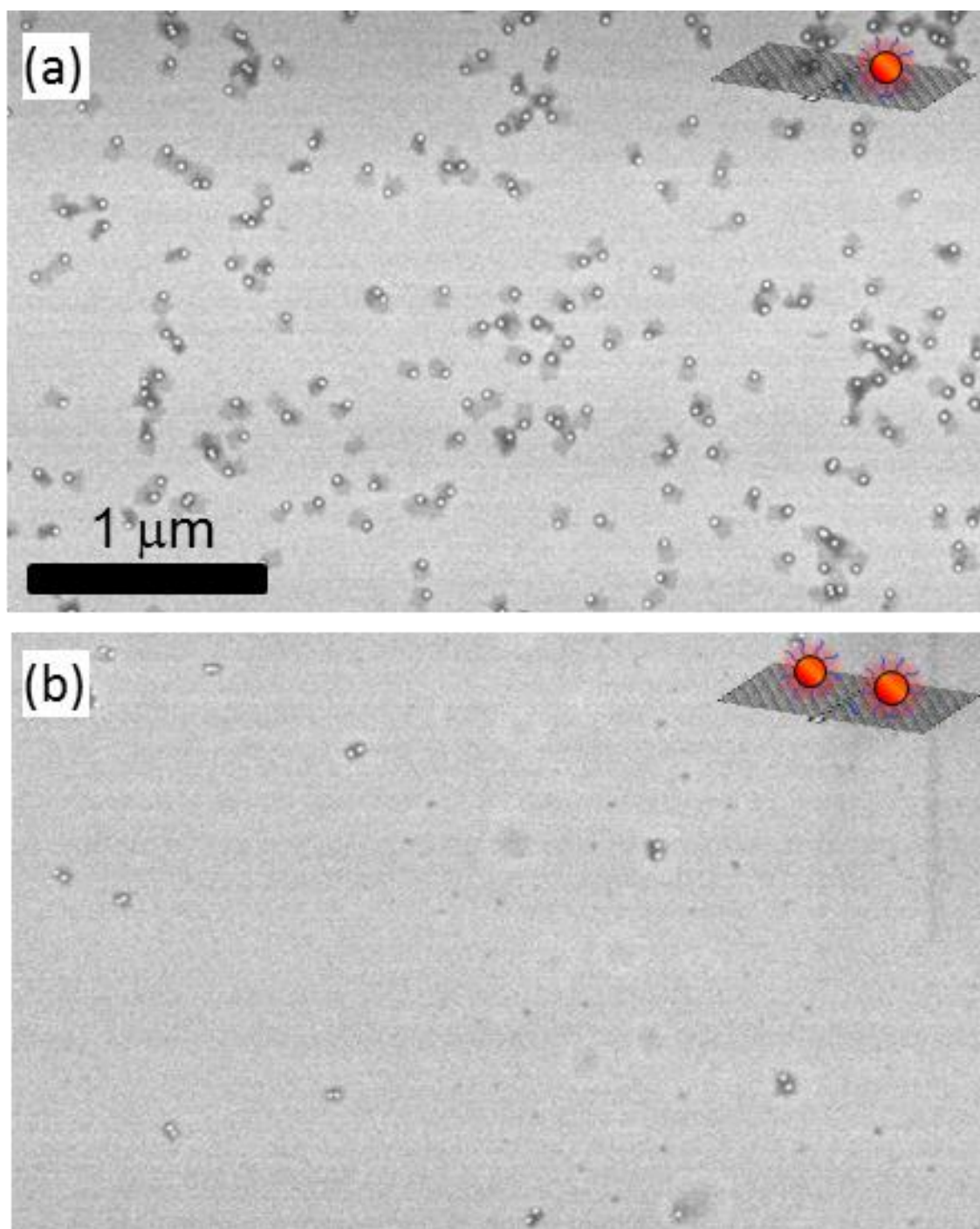


**Figure S14.** Typical SEM images of different fractions of  $n20$  nm AuNP-origami conjugates purified by centrifugation. The extracted fractions, f1 and f2 are 1AuNP-origami,  $(97.0 \pm 1.6)\%$  and 2AuNP-origami,  $(94.3 \pm 5.8)\%$ , respectively, as determined from an analysis of SEM images.

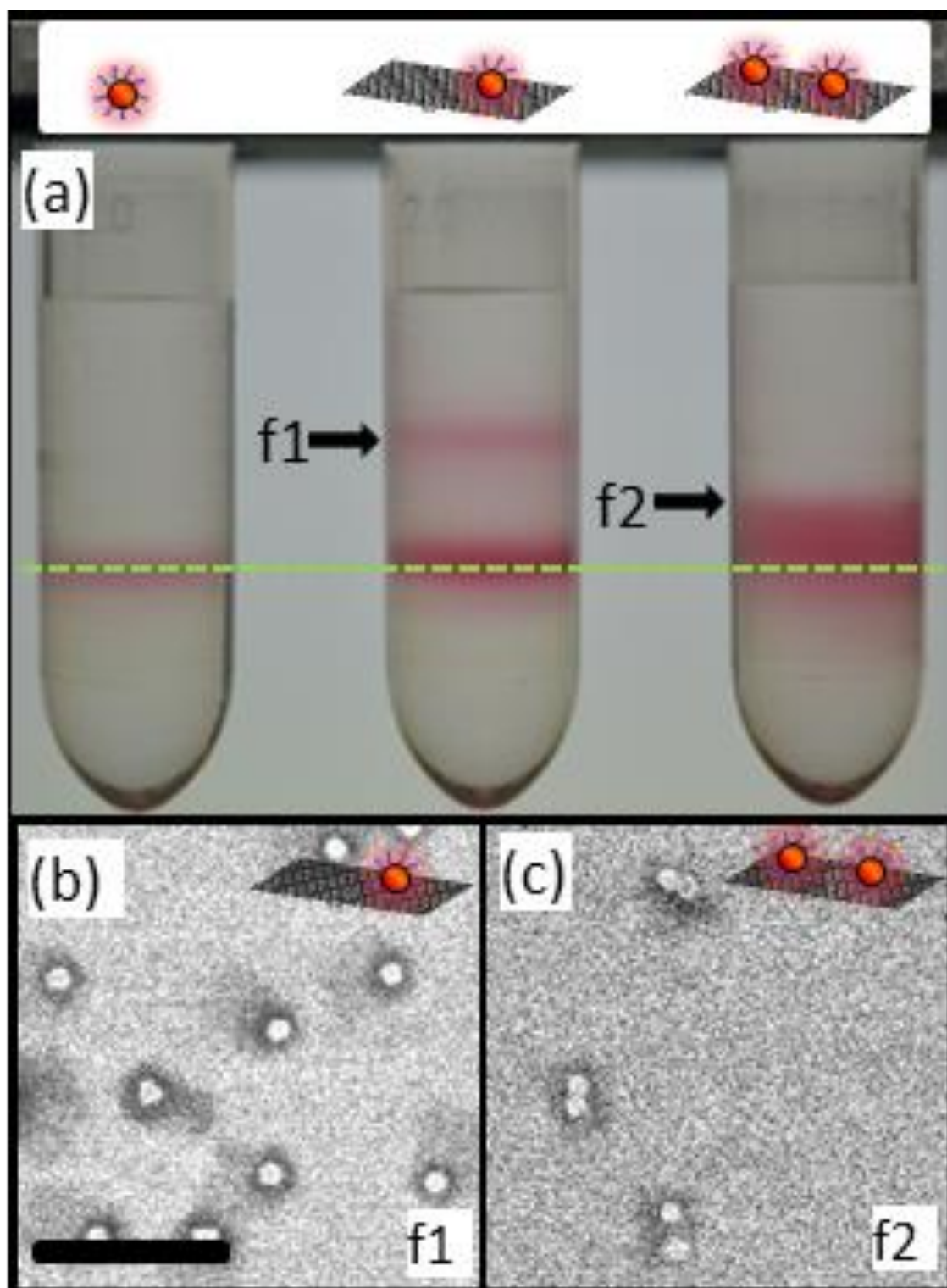


**Figure S15.** (a) Photograph of the centrifuge tubes containing  $n30$  nm AuNP-DNA origami after spinning for 2 h at  $287 \text{ rad s}^{-1}$  (2 740 rpm,  $7\,840 \text{ m s}^{-2}$ ,  $800 \times g$ ). (b)-(c) Typical SEM images of a fractions of AuNP-origami conjugates as labeled in (a).

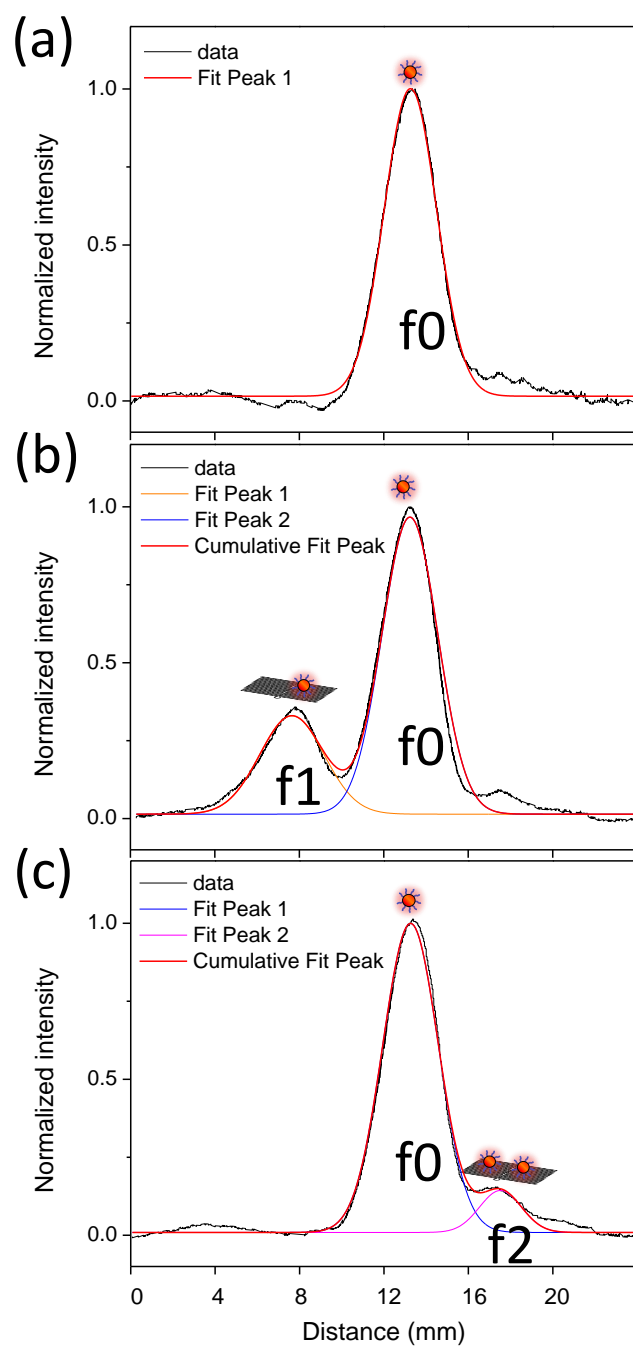


**Figure S16.** Centrifugam of  $n30$  nm AuNP-origami conjugates of each tube from the left to the right ((a) to (c)) in Figure S14 (a). Each band has been labeled as Figure S14 and fitted by a Gaussian function.

## Centrifugation Modeling Equations

We assume that AuNPs or  $n$ AuNP-origami ( $n$  is the number of AuNP bound to an origami) are isolated objects in solution, *i.e.*, “infinitely dilute solutions”, in which the objects experience only three forces during centrifugation in the reference frame of the centrifuge tube: a centrifugal force  $F_C$ , a buoyant force  $F_B$ , and a drag force  $F_D$ . The centrifugal force  $F_C$  is given by

$$F_C = m\omega^2 r, \quad (1)$$

where  $\omega$  is the angular velocity of the centrifuge,  $m$  is the mass of the object, and  $r$  is the distance of the object from the rotation axis. The buoyant force  $F_B$  is opposite in direction to the centrifugal force and is proportional to the mass  $m_0$  of fluid displaced by the object *via*<sup>[5]</sup>

$$F_B = -m_0\omega^2 r, \quad (2)$$

where  $\omega$  is the angular velocity and  $r$  is the distance of the object from the rotation axis. The drag force,  $F_D$  is expressed as the following,

$$F_D = -6\pi\eta_s R_H u \quad (3)$$

where  $u$  is the velocity of the object,  $\eta_s$  is the fluid viscosity, and  $R_H$  is the hydrodynamic radius of the object; collectively the terms  $6\pi\eta_s R_H$  are the drag coefficient for an object in a fluid medium.

Approximating,  $u = \frac{1}{2}(m-m_0)\omega^2 r t^2$ , and setting  $R_H$  proportional to  $a$ , the object radius, and  $(m-m_0)$  proportional to  $a^3$ , we see that the time taken to reach the terminal velocity is proportional to  $a/\sqrt{3\pi\eta}$ . Thus, for small objects, terminal velocity is reached in a very short time (less than  $10^{-6}$  s) during centrifugation, meaning that the object is always at its instantaneous terminal velocity throughout the separation medium. We therefore assume

$$F_C + F_B + F_D = 0, \quad (4)$$

which implies

$$u_t = \frac{(m - m_0)\omega^2 r}{6\pi\eta_s R_H}, \quad (5)$$

where  $u_t$  stands for terminal velocity.

Assuming that we know all of the quantities on the right-hand side of Equation (5), we may predict the total distance  $r_f$  that an object travels in during a fixed time interval by solving the equation

$$t = \int_{r_0}^{r_0+r_f} u_t^{-1}(r) dr, \quad (6)$$

where  $u_t^{-1}$  is the pace of the object (which depends on  $r$  via  $\eta_s$  and the fluid density  $\rho_{fluid}$ ),  $t$  is the total time the object is allowed to fall, and  $r_0$  is the initial position of the object relative to the axis of rotation. The physics of Equation (6) is straightforward: the time to travel a distance  $r_f$  is the sum over the infinitesimal paces of the object times the distance it travels at each pace. The difference in masses  $m - m_0$  can be written in the form

$$m - m_0 = V_{or}\Delta\rho_{or} + n(V_{au}\Delta\rho_{au} + V_{sh}\Delta\rho_{sh}), \quad (7)$$

where  $V_{or}$ ,  $V_{au}$ , and  $V_{sh}$  are the volumes of the DNA origami, AuNP, and DNA shell surrounding the AuNP, respectively; likewise, the  $\Delta\rho_{or}$ ,  $\Delta\rho_{au}$ , and  $\Delta\rho_{sh}$  are the densities of origami, AuNP, and shells surrounding the AuNP *relative* to the surrounding medium (i.e.,  $\Delta\rho_{or} = \rho_{or} - \rho_{fluid}$ , etc.). Combining Equation (5) – (7) gives

$$t = \int_{r_0}^{r_0+r_f} \frac{6\pi R_H \eta_s}{\omega^2 r [V_{or}\Delta\rho_{or} + n(V_{au}\Delta\rho_{au} + V_{sh}\Delta\rho_{sh})]} dr, \quad (8)$$

where  $\eta_s$  and the  $\Delta\rho$  depend on  $r$ .

In order to actually compute Equation (8), we assume that the AuNPs and DNA shells are spherical, which implies

$$V_{au} = \frac{4\pi a^3}{3} \quad (9)$$

$$V_{sh} = \frac{4\pi(a+a_d)^3}{3} - \frac{4\pi a^3}{3} \quad (10)$$

where  $a$  is the radius of the AuNP and  $a_d$  is the thickness of the DNA shell. We also take  $V_{or} = 14,000 \text{ nm}^3$  ( $100 \text{ nm} \times 70 \text{ nm} \times 2 \text{ nm}$ ) and assume that the fluid density and viscosity can be approximated as exponential functions of  $r$ . These are derived by first fitting the data in Table S1 to determine  $\eta$  and  $\rho$  as a function of iodixanol concentration and then fitting the values of  $\eta$  and  $\rho$  as a function of  $r$ . The integral in Equation (8) is computed numerically to find  $r_f$ .

The most significant sources of experimental error affecting this analytical model probably relate to uncertainties in the actual dynamic viscosity profile in the centrifuge tube. The principle sources for these are pipetting errors during the construction of the gradient, diffusion of the gradient prior to and during centrifugation, and temperature deviations from the set point during centrifugation.

### Band Width Analysis

We compute the widths of the sedimentation bands, which we assume to be approximately Gaussian, by calculating the sedimentation distances,  $r_f$ , for particles of radius  $\bar{a}$ ,  $(\bar{a} + \sigma)$  and  $(\bar{a} - \sigma)$ , where  $\bar{a}$  is the mean radius, and  $\sigma$  is the standard deviation in particle radius determined from TEM measurements. The normalized band width for each nanoparticle or construct is:

$$\frac{r_f(\bar{a} + \sigma) - r_f(\bar{a} - \sigma)}{r_f(\bar{a})} \quad (11)$$

The same procedure is followed for  $n$ AuNP-origami constructs, but we assume that the variations in AuNP size are uncorrelated, and therefore divide  $\sigma$  by  $\sqrt{n}$ , where  $n$  is 1, 2, or 3 to calculate the variation in the mass of nanoparticles attached to each construct. As noted in the main text, we assume a constant hydrodynamic radius,  $R_H$ , for all constructs equal to that measured by DLS for free origami.

Finally, we note that the absolute values of the measured and calculated distances do not agree. A sensitivity analysis of the possible sources of error suggests that the most probable cause of deviation is the likely difference between the actual and estimated dynamic viscosity profile along the centrifuge tube, as described above.

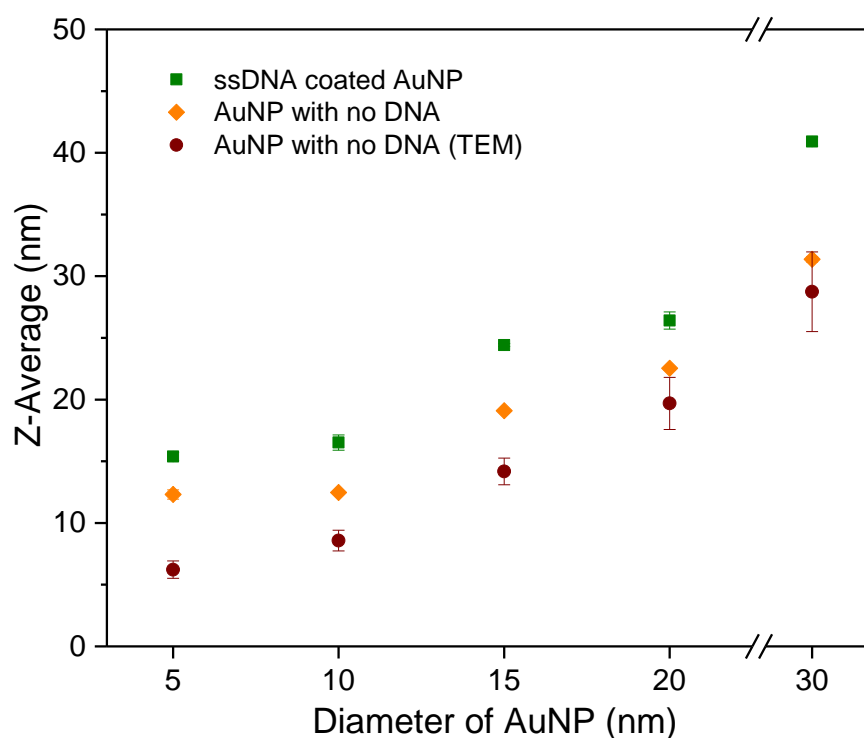


**Figure S17.** Diameter of AuNPs with or without a DNA coating measured by DLS and TEM. DLS measurements are performed in solution and report the hydrodynamic size of the particles. TEM measurements are performed in vacuum and quantify the size of the AuNPs alone, and are not sensitive to the presence of DNA or other surface functionalization. Vertical bars are one standard deviation.

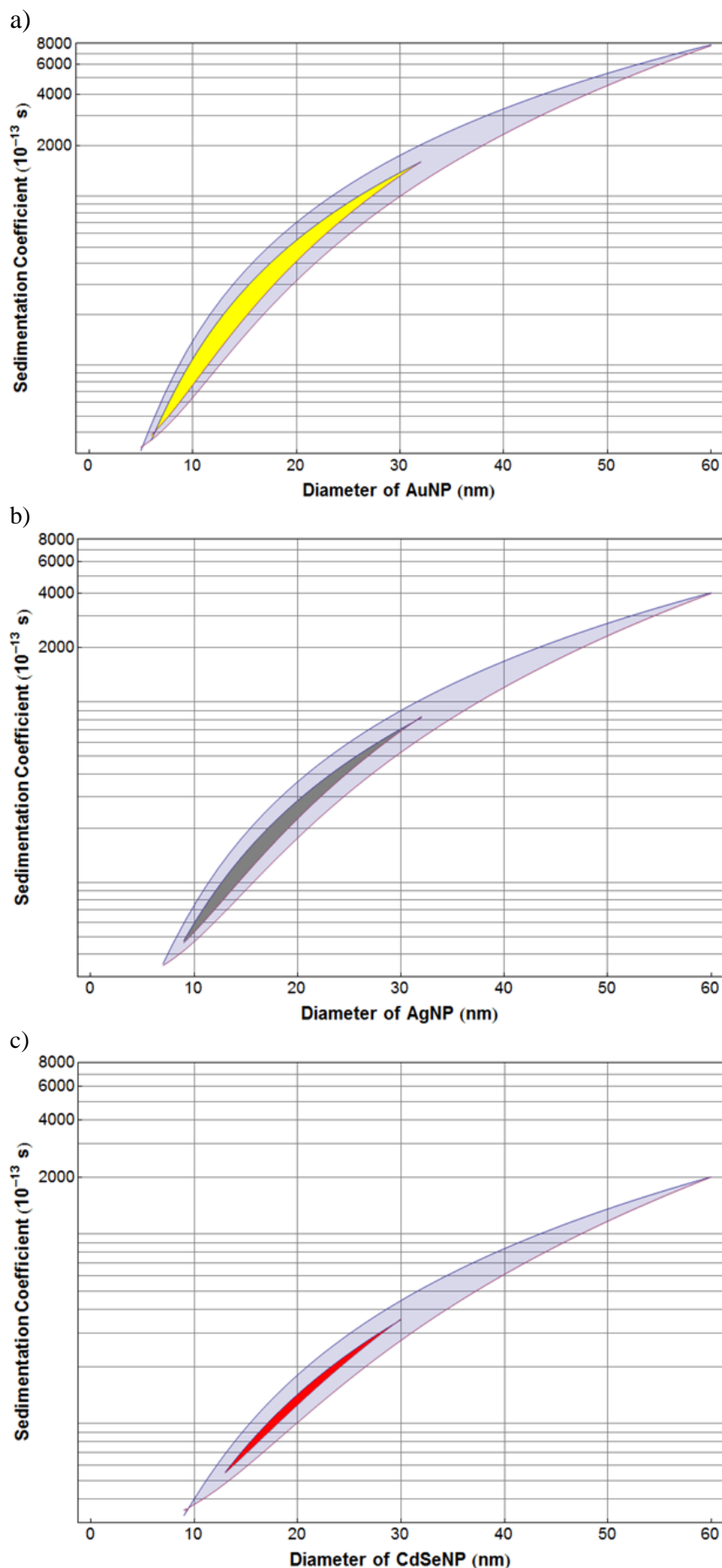


**Figure S18.** Comparison of sedimentation coefficients vs. particle size for free gold nanoparticles and 1AuNP-origami constructs, free silver nanoparticles and 1AgNP-origami constructs, and free CdSe nanoparticles and 1CdSeNP-origami constructs. The larger shaded area represents the range of particle sizes over which separations can be achieved, assuming a monodisperse size distribution. The small shaded area represents the range of particle sizes over which separations can be achieved, assuming a size distribution which varies by  $\pm 10\%$  about the average. As the nanoparticle density decreases, the nanoparticle size must increase in order to add appreciable mass and thus change the sedimentation coefficient of the NP-origami complex. The densities of the three materials are:  
 Au,  $19.3 \times 10^3 \text{ kg m}^{-3}$ ;  
 Ag,  $10.5 \times 10^3 \text{ kg m}^{-3}$ ;  
 CdSe,  $5.8 \times 10^3 \text{ kg m}^{-3}$

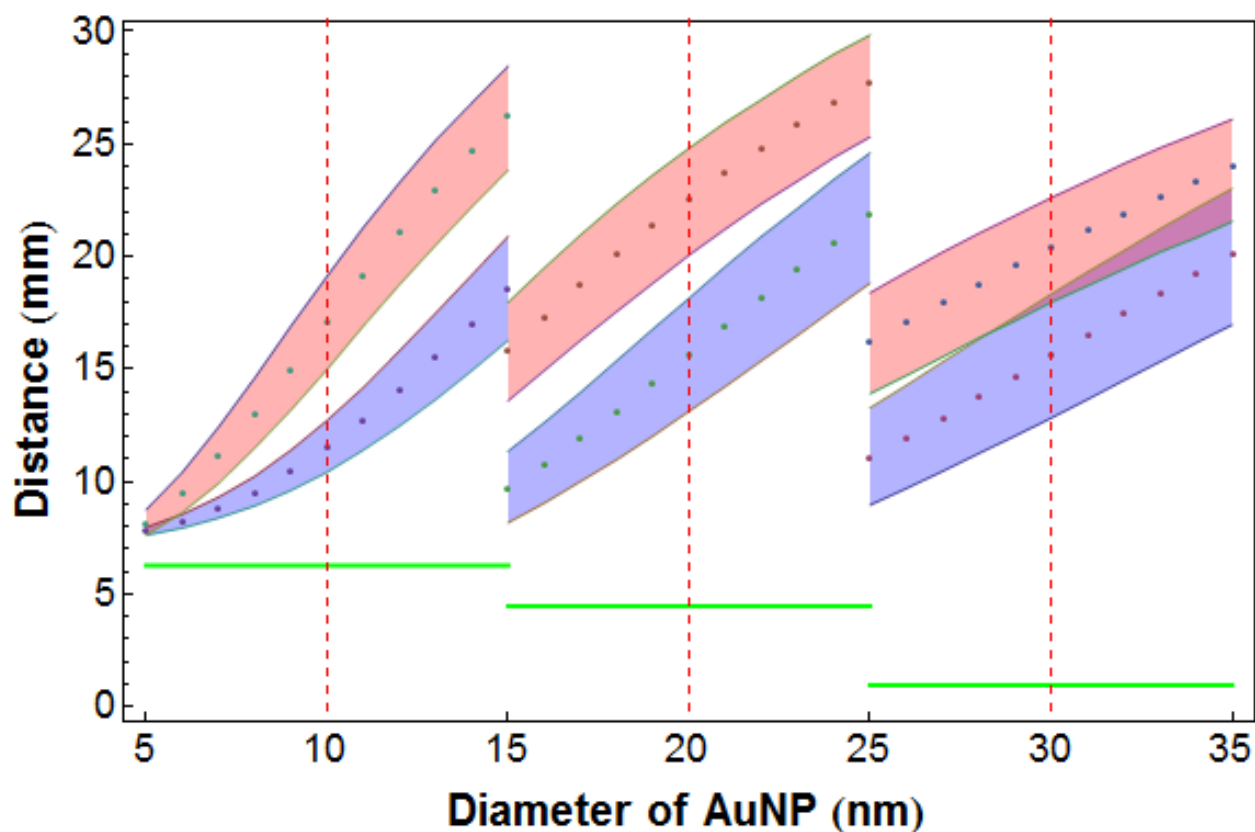


**Figure S19.** Sedimentation distance versus particle size for free gold nanoparticles and 1AuNP-origami constructs. The red bands represent the distance traveled by free gold nanoparticles assuming a nanoparticle size variation of  $\pm 10\%$ , and the blue bands the distance traveled by 1AuNP-origami constructs. The horizontal green lines are the distances traveled by undecorated origami.

## References

1. P. W. K. Rothmund, *Nature*, 2006, **440**, 302.
2. S. Pal, Z. Deng, B. Ding, H. Yan, Y. Liu, *Angew. Chem. Int. Ed.*, **2010**, 49, 2704.
3. F. C. Klebaner, *Introduction to Stochastic Calculus with Applications (Second Edition)*, Imperial College Press, London, England **2005**.

**Sequence of single stranded M13mp18** can be found at the website of New England

BioLabs Inc.;

<https://www.neb.com/~media/NebUs/Page%20Images/Tools%20and%20Resources/Interactive%20Tools/DNA%20Sequences%20and%20Maps/Text%20Documents/m13mp18gbk.txt>

### Sequences of unmodified & modified staple strands

In order to capture T18 coated AuNPs, specific staple strands at pre-determined locations were extended with 22 Adenines. The following strands are the modified strands at different binding sites.

14, 61, 85, 87, 119, 121, 145, 147, 171

T18 strand: 5'-/5DTPA/TTT TTT TTT TTT TTT TTT TTT -3'

**Table S2.** Sequences of unmodified staple strands

Name	Sequence (5' → 3')
1	CAAGCCCAATAGGAAC CCATGTACAAACAGTT
2	AATGCCCGTAAACAGT GCCCGTATCTCCCTCA
3	TGCCTTGACTGCCTAT TTCGGAACAGGGATAG
4	GAGCCGCCCCACCACC GGAACCGCGACGGAAA
5	AACCAGAGACCCTCAG AACCGCCAGGGGTCAG
6	TTATTCATAGGGAAGG TAAATATT CATTTCAGT
7	CATAACCCGAGGCATA GTAAGAGC TTTTAAAG
8	ATTGAGGGTAAAGGTG AATTATCAATCACCGG
9	AAAAGTAATATCTTAC CGAAGCCCTTCCAGAG
10	GCAATAGCGCAGATAG CCGAACAATTCAACCG
11	CCTAATTTACGCTAAC GAGCGTCTAATCAATA
12	TCTTACCAGCCAGTTA CAAAATAAATGAAATA
13	ATCGGCTGCGAGCATG TAGAAACCTATCATAT
14	CTAATTTATCTTTCCT TATCATTATCCTGAA
15	GCGTTATAGAAAAAGC CTGTTTATAG AAGGCCGG
16	GCTCATTTTTCGCATTAA AATTTTTG AGCTTAGA
17	AATTACTACAAATTCT TACCAGTAATCCCATC
18	TTAAGACGTTGAAAAC ATAGCGATAACAGTAC
19	TAGAATCCCTGAGAAG AGTCAATAGGAATCAT
20	CTTTTACACAGATGAA TATACAGTAAACAATT
21	TTTAACGTTTCGGGAGA AACAATAATTTTCCCT
22	CGACAATAAGTATTA GACTTTACAATACCGA
23	GGATTTAGCGTATTAA ATCCTTTGTTTTCAGG
24	ACGAACCAAAACATCG CCATTTAA TGGTGGTT
25	GAACGTGGCGAGAAAG GAAGGGAA CAAACTAT
26	TAGCCCTACCAGCAGA AGATAAAAACATTTGA
27	CGGCCTTGCTGGTAAT ATCCAGAACGAACCTGA
28	CTCAGAGCCACCACCC TCATTTTCTATTATT
29	CTGAAACAGGTAATAA GTTTTAAACCCCTCAGA
30	AGTGTACTTGAAAGTA TTAAGAGGCCGCCACC
31	GCCACCACTCTTTTCA TAATCAAACCGTCACC

32	GTTTGCCACCTCAGAG CCGCCACCGATACAGG
33	GACTTGAGAGACAAAA GGGCGACAAGTTACCA
34	AGCGCCAACCATTTGG GAATTAGATTATTAGC
35	GAAGGAAAATAAGAGC AAGAAACAACAGCCAT
36	GCCCAATACCGAGGAA ACGCAATAGGTTTACC
37	ATTATTTAACCAGCT ACAATTTTCAAGAACG
38	TATTTTGCTCCCAATC CAAATAAGTGAGTTAA
39	GGTATTAAGAACAAGA AAAATAATTAAGCCA
40	TAAGTCCTACCAAGTA CCGCACTCTTAGTTGC
41	ACGCTCAAATAAGAA TAAACACCGTGAATTT
42	AGGCGTTACAGTAGGG CTTAATTGACAATAGA
43	ATCAAAATCGTCGCTA TTAATTAACGGATTTCG
44	CTGTAAATCATAGGTC TGAGAGACGATAAATA
45	CCTGATTGAAAGAAAT TGCGTAGACCCGAACG
46	ACAGAAATCTTTGAAT ACCAAGTTCCTTGCTT
47	TTATTAATGCCGTCAA TAGATAATCAGAGGTG
48	AGATTAGATTTAAAAG TTTGAGTACACGTAAA
49	AGGCGGTCATTAGTCT TTAATGCGCAATATTA
50	GAATGGCTAGTATTAA CACCGCCTCAACTAAT
51	CCGCCAGCCATTGCAA CAGGAAAAATATTTTT
52	CCCTCAGAACCGCCAC CCTCAGAACTGAGACT
53	CCTCAAGAATACATGG CTTTTGATAGAACCAC
54	TAAGCGTCGAAGGATT AGGATTAGTACCGCCA
55	CACCAGAGTTCGGTCA TAGCCCCCGCCAGCAA
56	TCGGCATTCCGCCGCC AGCATTGACGTTCCAG
57	AATCACCAATAGAAA ATTCATATATAACGGA
58	TCACAATCGTAGCACC ATTACCATCGTTTTCA
59	ATACCCAAGATAACCC ACAAGAATAAACGATT
60	ATCAGAGAAAGAACTG GCATGATTTTATTTTG
61	TTTTGTTAAGCCTTA AATCAAGAATCGAGAA
62	AGGTTTTGAACGTCAA AAATGAAAGCGCTAAT
63	CAAGCAAGACGCGCCT GTTTATCAAGAATCGC
64	AATGCAGACCGTTTTT ATTTTCATCTTGCGGG
65	CATATTTAGAAATACC GACCGTGTTACCTTTT
66	AATGGTTTACAACGCC AACATGTAGTTCAGCT
67	TAACCTCCATATGTGA GTGAATAAACAAAATC
68	AAATCAATGGCTTAGG TTGGGTTACTAAATTT
69	GCGCAGAGATATCAA ATTATTTGACATTATC
70	AACCTACCGCGAATTA TTCATTTCCAGTACAT
71	ATTTTGCGTCTTTAGG AGCACTAAGCAACAGT
72	CTAAAATAGAACAAAG AAACCACCAGGGTTAG
73	GCCACGCTATACGTGG CACAGACAACGCTCAT
74	GCGTAAGAGAGAGCCA GCAGCAAAAAGGTTAT
75	GGAAATACCTACATTT TGACGCTCACCTGAAA
76	TATCACCGTACTCAGG AGGTTTAGCGGGGTTT
77	TGCTCAGTCAGTCTCT GAATTTACCAGGAGGT
78	GGAAAGCGACCAGGCG GATAAGTGAATAGGTG
79	TGAGGCAGGCGTCAGA CTGTAGCGTAGCAAGG
80	TGCCTTTAGTCAGACG ATTGGCCTGCCAGAAT
81	CCGGAACACACCACG GAATAAGTAAGACTCC
82	ACGCAAAGGTCACCAA TGAAACCAATCAAGTT
83	TTATTACGGTCAGAGG GTAATTGAATAGCAGC

84	TGAACAAACAGTATGT TAGCAAACATAAAAGAA
85	CTTTACAGTTAGCGAA CCTCCCGACGTAGGAA
86	GAGGCGTTAGAGAATA ACATAAAAGAACACCC
87	TCATTACCCGACAATA AACACATATTTAGGC
88	CCAGACGAGCGCCCAA TAGCAAGCAAGAACGC
89	AGAGGCATAATTTTCAT CTTCTGACTATAACTA
90	TTTTAGTTTTTTTCGAGC CAGTAATAAATTCTGT
91	TATGTAAACCTTTTTT AATGGAAAATTACCT
92	TTGAATTATGCTGATG CAAATCCACAAATATA
93	GAGCAAAAACCTTCTGA ATAATGGAAGAAGGAG
94	TGGATTATGAAGATGA TGA AACAAAATTTTCAT
95	CGGAATTATTGAAAGG AATTGAGGTGAAAAAT
96	ATCAACAGTCATCATA TTCCTGATTGATTGTT
97	CTAAAGCAAGATAGAA CCCTTCTGAATCGTCT
98	GCCAACAGTCACCTTG CTGAACCTGTTGGCAA
99	GAAATGGATTATTTAC ATTGGCAGACATTCTG
100	TTTT TATAAGTA TAGCCCGGCCGTCGAG
101	AGGGTTGA TTTT ATAAATCC TCATTAATGATATTC
102	ACAAACAA TTTT AATCAGTA GCGACAGATCGATAGC
103	AGCACCGT TTTT TAAAGGTG GCAACATAGTAGAAAA
104	TACATACA TTTT GACGGGAG AATTAACACAGGGAA
105	GCGCATT TTTT GCTTATCC GGTATTCTAAATCAGA
106	TATAGAAG TTTT CGACAAAA GGTAAAGTAGAGAATA
107	TAAAGTAC TTTT CGCGAGAA AACTTTTTATCGCAAG
108	ACAAAGAA TTTT ATTAATTA CATTAAACACATCAAG
109	AAAACAAA TTTT TTCATCAA TATAATCCTATCAGAT
110	GATGGCAA TTTT AATCAATA TCTGGTCACAAATATC
111	AAACCCTC TTTT ACCAGTAA TAAAGGGATTCACCA GTCACACGTTTT
112	CCGAAATCCGAAAATC CTGTTTGAAGCCGGAA
113	CCAGCAGGGGCAAAAT CCCTTATAAAGCCGGC
114	GCATAAAGTTCCACAC AACATACGAAGCGCCA
115	GCTCACAATGTAAAGC CTGGGGTGGGTTTGCC
116	TTCCGATTGCCGGAA ACCAGGCATTAATCA
117	GCTTCTGGTCAGGCTG CGCAACTGTGTTATCC
118	GTTAAATTTTAACCA ATAGGAACCCGGCACC
119	AGACAGTCATTCAAAA GGGTGAGAAGCTATAT
120	AGGTAAAGAAATCACC ATCAATATAATATTTT
121	TTTCATTTGGTCAATA ACCTGTTTATATCGCG
122	TCGCAAATGGGGCGCG AGCTGAAATAATGTGT
123	TTTTAATTGCCGAAA GACTTCAAACACTAT
124	AAGAGGAACGAGCTTC AAAGCGAAGATACATT
125	GGAATTACTCGTTTAC CAGACGACAAAAGATT
126	GAATAAGGACGTAACA AAGCTGCTCTAAAACA
127	CCAAATCACTTGCCCT GACGAGAACGCCAAAA
128	CTCATCTTGAGGCAAA AGAATACAGTGAATTT
129	AAACGAAATGACCCCC AGCGATTATTCATTAC
130	CTTAAACATCAGCTTG CTTTCGAGCGTAACAC
131	TCGGTTTAGCTTGATA CCGATAGTCCAACCTA
132	TGAGTTTCGTCACCAG TACAACTTAATTGTA
133	CCCCGATTTAGAGCTT GACGGGGAAATCAAAA
134	GAATAGCCGCAAGCGG TCCACGCTCCTAATGA
135	GAGTTGCACGAGATAG GGTTGAGTAAGGGAGC

136	GTGAGCTAGTTTCCTG TGTGAAATTTGGGAAG
137	TCATAGCTACTCACAT TAATTGCGCCCTGAGA
138	GGCGATCGCACTCCAG CCAGCTTTGCCATCAA
139	GAAGATCGGTGCGGGC CTCTTCGCAATCATGG
140	AAATAATTTTAAATTG TAAACGTTGATATTCA
141	GCAAAATATCGCGTCTG GCCTTCCTGGCCTCAG
142	ACCGTTCTAAATGCAA TGCCTGAGAGGTGGCA
143	TATATTTTAGCTGATA AATTAATGTTGTATAA
144	TCAATTCTTTTAGTTT GACCATTACCAGACCG
145	CGAGTAGAACTAATAG TAGTAGCAAACCCTCA
146	GAAGCAAAAAAGCGGA TTGCATCAGATAAAAA
147	TCAGAAGCCTCCAACA GGTCAGGATCTGCGAA
148	CCAAAATATAATGCAG ATACATAAACACCAGA
149	CATTCAACGCGAGAGG CTTTTGCATATTATAG
150	ACGAGTAGTGACAAGA ACCGGATATACCAAGC
151	AGTAATCTTAAATTGG GCTTGAGAGAATACCA
152	GCGAAACATGCCACTA CGAAGGCATGCGCCGA
153	ATACGTAAGTACAA CGGAGATTTTCATCAAG
154	CAATGACACTCCAAAA GGAGCCTTACAACGCC
155	AAAAAAGGACAACCAT CGCCCACGCGGGTAAA
156	TGTAGCATTCCACAGA CAGCCCTCATCTCCAA
157	GTAAGCACTAAATCG GAACCCTAGTTGTTCC
158	AGTTTGGAGCCCTTCA CCGCCTGGTTGCGCTC
159	AGCTGATTACAAGAGT CCACTATTGAGGTGCC
160	ACTGCCCGCCGAGCTC GAATTCGTTATTACGC
161	CCCGGGTACTTTCCAG TCGGGAAACGGGCAAC
162	CAGCTGGCGGACGACG ACAGTATCGTAGCCAG
163	GTTTGAGGGAAAGGGG GATGTGCTAGAGGATC
164	CTTTCATCCCCAAAAA CAGGAAGACCGGAGAG
165	AGAAAAGCAACATTAA ATGTGAGCATCTGCCA
166	GGTAGCTAGGATAAAA ATTTTTAGTTAACATC
167	CAACGCAATTTTTGAG AGATCTACTGATAATC
168	CAATAAATACAGTTGA TTCCAATTTAGAGAG
169	TCCATATACATACAGG CAAGGCAACTTTATTT
170	TACCTTTAAGGTCTTT ACCCTGACAAAGAAGT
171	CAAAAATCATTGCTCC TTTTGATAAGTTTCAT
172	TTTGCCAGATCAGTTG AGATTTAGTGGTTTAA
173	AAAGATTCAGGGGGTA ATAGTAAACCATAAAT
174	TTTCAACTATAGGCTG GCTGACCTTGATCAT
175	CCAGGCGCTTAATCAT TGTGAATTACAGGTAG
176	CGCCTGATGGAAGTTT CCATTAACATAACCG
177	TTTCATGAAAATTGTG TCGAAATCTGTACAGA
178	ATATATTCTTTTTTCA CGTTGAAAATAGTTAG
179	AATAATAAGGTCGCTG AGGCTTGCAAAGACTT
180	CGTAACGATCTAAAGT TTTGTCGTGAATTGCG
181	ACCCAAATCAAGTTTT TTGGGGTCAAAGAACG
182	TGGACTCCCTTTTCAC CAGTGAGACCTGTCTG
183	TGGTTTTTAACGTCAA AGGGCGAAGAACCATC
184	GCCAGCTGCCTGCAGG TCGACTCTGCAAGGCG
185	CTTGCATGCATTAATG AATCGGCCCGCCAGGG
186	ATTAAGTTCGCATCGT AACCGTGCGAGTAACA
187	TAGATGGGGGGTAACG CCAGGGTTGTGCCAAG

188	ACCCGTCGTCATATGT ACCCCGGTAAAGGCTA
189	CATGTCAAGATTCTCC GTGGGAACCGTTGGTG
190	TCAGGTCACCTTTTGCG GGAGAAGCAGAATTAG
191	CTGTAATATTGCCTGA GAGTCTGGAAAAGTAG
192	CAAAATTAAGTACGG TGTCTGGAAGAGGTCA
193	TGCAACTAAGCAATAA AGCCTCAGTTATGACC
194	TTTTTGCGCAGAAAAC GAGAATGAATGTTTAG
195	AAACAGTTGATGGCTT AGAGCTTATTTAATA
196	ACTGGATAACGGAACA ACATTATTACCTTATG
197	ACGAACTAGCGTCCAA TACTGCGGAATGCTTT
198	CGATTTTAGAGGACAG ATGAACGGCGCGACCT
199	CTTTGAAAAGAACTGG CTCATTATTTAATAAA
200	GCTCCATGAGAGGCTT TGAGGACTAGGGAGTT
201	ACGGCTACTTACTTAG CCGGAACGCTGACCAA
202	AAAGGCCGAAAGGAAC AACTAAAGCTTTCCAG
203	GAGAATAGCTTTTGCG GGATCGTCGGGTAGCA
204	ACGTTAGTAAATGAAT TTTCTGTAAGCGGAGT
205	TTTT CGATGGCC CACTACGTAAACCGTC
206	TATCAGGG TTTT CGGTTTGC GTATTGGGAACGCGCG
207	GGGAGAGG TTTT TGTA AAC GACGGCCATTCCCAGT
208	CACGACGT TTTT GTAATGGG ATAGGTCAAACGGCG
209	GATTGACC TTTT GATGAACG GTAATCGTAGCAAACA
210	AGAGAATC TTTT GGTTGTAC CAAAACAAGCATAAA
211	GCTAAATC TTTT CTGTAGCT CAACATGTATTGCTGA
212	ATATAATG TTTT CATTGAAT CCCCTCAAATCGTCA
213	TAAATATT TTTT GGAAGAAA AATCTACGACCAGTCA
214	GGACGTTG TTTT TCATAAGG GAACCGAAAGGCGCAG
215	ACGGTCAA TTTT GACAGCAT CGGAACGAACCCTCAG
216	CAGCGAAAA TTTT ACTTTCA ACAGTTTCTGGGATTT TGCTAAAC TTTT
Loop1	AACATCACTTGCCTGAGTAGAAGAACT
Loop2	TGTAGCAATACTTCTTTGATTAGTAAT
Loop3	AGTCTGTCCATCACGCAAATTAACCGT
Loop4	ATAATCAGTGAGGCCACCGAGTAAAAG
Loop5	ACGCCAGAATCCTGAGAAGTGTTTTT
Loop6	TTAAAGGGATTTTAGACAGGAACGGT
Loop7	AGAGCGGGAGCTAACAGGAGGCCGA
Loop8	TATAACGTGCTTTCCTCGTTAGAATC
Loop9	GTACTATGGTTGCTTTGACGAGCACG
Loop10	GCGCTTAATGCGCCGCTACAGGGCGC